# Coseismic magnetization of fault pseudotachylytes: 1. Thermal demagnetization experiments

E. C. Ferre, J. Geissman, François Demory, J. Gattacceca, M. Zechmeister, M. Hill

AGU PUBLICATIONS

JGR

Journal of Geophysical Research: Solid Earth

RESEARCH ARTICLE
10.1002/2014JB011168

**Key Points:**
- Fault pseudotachylytes hold NRM unrelated to the geomagnetic field
- Fault pseudotachylytes hold a multicomponent NRM

**Correspondence to:**
E. C. Ferré,
eferre@geo.siu.edu

**Citation:**
Ferré, E. C., J. W. Geissman, F. Demory, J. Gattacceca, M. S. Zechmeister, and M. J. Hill (2014), Coseismic magnetization of fault pseudotachylytes: 1. Thermal demagnetization experiments, *J. Geophys. Res. Solid Earth*, *119*, 6113–6135, doi:10.1002/2014JB011168.

Received 4 APR 2014
Accepted 10 JUL 2014
Accepted article online 15 JUL 2014
Published online 6 AUG 2014

# Coseismic magnetization of fault pseudotachylytes: 1. Thermal demagnetization experiments

**E. C. Ferré[1], J. W. Geissman[2], F. Demory[3], J. Gattacceca[3], M. S. Zechmeister[4], and M. J. Hill[5]**

[1]Department of Geology, Southern Illinois University, Carbondale, Illinois, USA, [2]Department of Geosciences, University of Texas at Dallas, Richardson, Texas, USA, [3]CNRS, Aix-Marseille Université, CEREGE-UMR7330, Aix-en-Provence, France, [4]SEPCO, EPX-X Alaska, Houston, Texas, USA, [5]Department of Earth, Ocean and Ecological Sciences, University of Liverpool, Liverpool, UK

**Abstract** Fault pseudotachylytes form by quenching of silicate liquids produced through coseismic frictional melting. Here we show that in natural pseudotachylytes the main carrier of magnetic remanence blocked in during cooling of the frictional melt is fine-grained magnetite. This confirms previous studies on friction melt experiments. Stoichiometric magnetite, produced during earthquakes by the breakdown of ferromagnesian silicates, records the ambient magnetic field during seismic slip. We find that most fault pseudotachylytes exposed in the Santa Rosa Mountains, southern California, a classic pseudotachylyte locality, acquired their natural remanent magnetization (NRM) upon cooling of the frictional melt through the range of magnetization blocking temperatures of the magnetite grains and this primarily constitutes a thermal remanent magnetization. NRM intensities typical of most pseudotachylyte veins range from 1 to $60{\cdot}10^{-4}$ $Am^2/kg$. A few specimens, however, contain magnetizations significantly higher than that caused by the Earth's field as well as magnetization directions that are highly variable over short distances. Other magnetization processes, possibly related to coseismic electric currents, may be involved during the seismogenic process to control NRM acquisition.

## 1. Introduction

Fault pseudotachylytes, generally viewed as earthquake fossils [*Andersen and Austrheim*, 2006; *Lin*, 2008], may hold clues to the physics of seismic slip [e.g., *Austrheim and Boundy*, 1994; *Di Toro et al*., 2005; *Ueda et al*., 2008; *Del Gaudio et al*., 2009; *Janssen et al*., 2010; *Niemeijer et al*., 2013]. These rocks form by rapid rise in temperature along the slip plane due to friction, followed by melting and fast cooling [*Magloughlin*, 1992; *Di Toro et al*., 2005; *Ferré et al*., 2005a; *Abercrombie et al*., 2006; *Andersen and Austrheim*, 2006; *Kirkpatrick et al*., 2009; *Lin*, 2011; *Spray*, 2011; *Chou et al*., 2012].

Frictional melts solidify and cool very fast and may, like volcanic glasses, constitute excellent paleointensity recorders [*Nakamura et al*., 2002; *Ferré et al*., 2005b, 2012]. Early paleomagnetic studies of fault pseudotachylytes interpreted the natural remanent magnetization (NRM) of pseudotachylytes as a thermal remanent magnetization (TRM) acquired primarily by ferrimagnetic (magnetite, maghemite) grains upon cooling [*Piper*, 1981; *Piper and Poppleton*, 1988]. Yet recent investigations on active faults show that a chemical remanent magnetization (CRM), carried by hematite or goethite, could also contribute to NRM [*Fukuchi*, 2003; *Fukuchi et al*., 2005; *Hirono et al*., 2006; *Chou et al*., 2012]. Although TRM acquisition must occur during and shortly after seismic slip, due to melt quenching, the timing of CRM acquisition remains generally poorly determined [*Molina Garza et al*., 2009]. Finally, earthquake lightning may constitute an additional magnetization process [e.g., *Enomoto and Zheng*, 1998; *Ferré et al*., 2005b].

In this study, we investigate the magnetization processes and the estimated intensity of magnetic fields associated with the formation and alteration of fault pseudotachylytes. The specimens come from the well-researched Santa Rosa Mountains locality, Peninsular Coastal Ranges, California [*Wenk et al*., 2000; *Ferré et al*., 2005b, 2012]. The first part of this study of the remanence in these rocks focuses on thermal demagnetization of NRM experiments (including selected microwave demagnetization experiments) with the aim to decipher magnetization acquisition processes. The second part reports on alternating field NRM demagnetization experiments with the aim of quantifying coseismic field intensity.

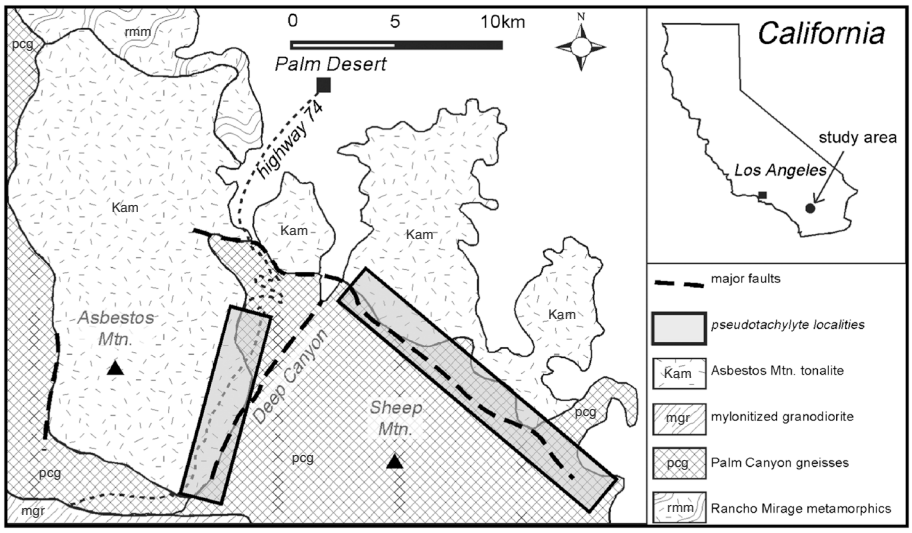


**Figure 1.** Simplified geologic map showing the location of the two sampling sites in the Santa Rosa Mountains, California [after *Wenk et al*., 2000]. Both localities are located near major faults, yet the pseudotachylytes are not directly associated with the fault plane.

## 2. Previous Magnetic Studies on Fault and Artificial Pseudotachylytes

The Precambrian Ikertôq pseudotachylytes in Greenland hold a stable, single-component NRM interpreted as the coseismic record of the geomagnetic field [*Piper*, 1981]. In contrast, the NRM of the Angmagssalik pseudotachylytes, also from Greenland, was interpreted as having been acquired long after their cooling [*Beckmann*, 1982]. In a subsequent study, *Piper and Poppleton* [1988] attributed the multiple NRM components of the Lewisian pseudotachylytes in Scotland to successive slip events. These early studies consistently reported high Koenigsberger ratios ($Q_n$, the ratio of remanent magnetization to induced magnetization), from 10 to 100, and a magnetic remanence carried chiefly by single-domain (SD) to pseudo-single-domain (PSD) magnetite grains [*Piper and Poppleton*, 1988].

In contrast with these pioneering works, recent investigations on the active faults of Nojima in Japan [*Fukuchi*, 2003; *Fukuchi et al*., 2005] and Chelungpu in Taiwan [*Hirono et al*., 2006; *Chou et al*., 2012] revealed a more complex magnetic assemblage. For example, in the case of the Nojima fault, thermal dehydration of lepidocrocite ($\gamma$-FeOOH) in the sedimentary protolith resulted in maghemite ($\gamma$-$Fe_2O_3$) formation in the pseudotachylyte [*Fukuchi*, 2003]. In the Chelungpu pseudotachylyte, stoichiometric magnetite ($Fe_3O_4$), both inherited from the sedimentary protolith and neoformed during seismic slip, carries the NRM [*Chou et al*., 2012]. The surrounding Chelungpu fault gouge hosts goethite ($\alpha$-FeOOH) that formed after slip [*Chou et al*., 2012]. In the unaltered pseudotachylytes of the Santa Rosa Mountains in California, the NRM is primarily carried by pseudo-single-domain (PSD) magnetite, although oxidized pseudotachylyte veins have a secondary NRM component carried by hematite ($\alpha$-$Fe_2O_3$) [*Ferré et al*., 2005b, 2012]. Finally, the pseudotachylytes from the Chiapas Massif in Mexico formed from a hematite-bearing quartz-diorite protolith and show a relatively moderate NRM carried mainly by PSD magnetite and minor amounts of maghemite and hematite [*Molina Garza et al*., 2009]. In the Chiapas pseudotachylytes, the NRM is interpreted as a magnetite-born TRM overprinted by a CRM carried by hematite and goethite.

The friction experiments of *Nakamura et al*. [2002] shed light on the nature of primary magnetic phases in pseudotachylytes. Because the pseudotachylyte veins were made in the laboratory, they are free of any alteration product and must therefore represent a pristine magnetic assemblage. Using two granite cylinders at velocity of 1.5 m $s^{-1}$ under 1.5 MPa normal stress and ambient atmosphere conditions, *Nakamura et al*. [2002] fabricated pseudotachylytes with an NRM carried by single-domain to PSD grains of stoichiometric magnetite. This magnetite formed through breakdown of hornblende and biotite.

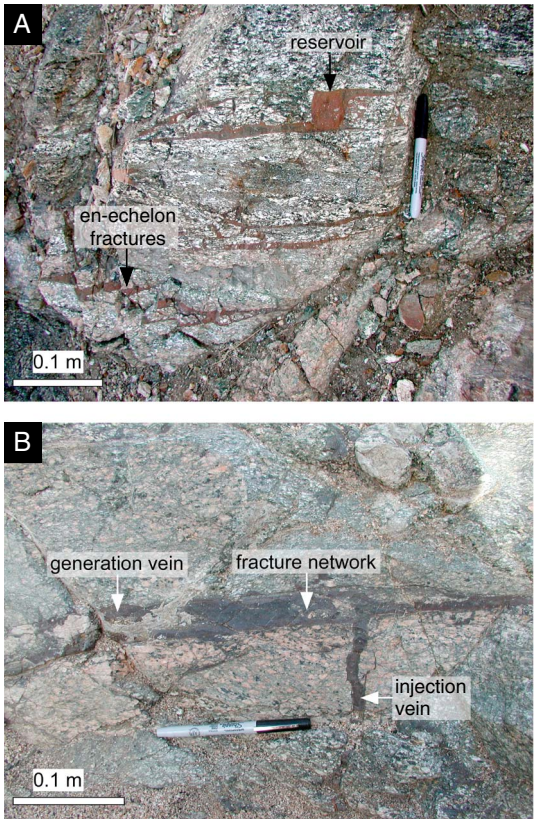


**Figure 2.** Outcrop-scale geometric features of the pseudotachylyte veins at Santa Rosa. (a) Multiple parallel generation veins, en echelon fractures, and "pull-apart"-shaped reservoir vein, all subparallel to foliation in the host Palm Canyon complex gneisses, Deep Canyon area. (b) Generation vein, fracture network, and injection vein in Devil Canyon area.

In summary, previous studies emphasize that the nature of the magnetic phase carrying the NRM depends on the pseudotachylyte protolith and that a postseismic magnetization may be imparted through oxidation of magnetite. This conclusion underlines the fact that in order to isolate coseismic magnetization acquisition mechanisms, it is necessary to perform paleomagnetic experiments on the least altered possible material.

## 3. Field and Macroscopic Characteristics of the Santa Rosa Pseudotachylytes

The Santa Rosa Mountains located in the Eastern Peninsular Ranges, 150 km east of Los Angeles, California (Figure 1), provide excellent pseudotachylyte exposures [*Wenk et al.*, 2000; *Ferré et al.*, 2005b, 2012]. These mountains consist of high-grade metamorphic complexes, such as the Palm Canyon gneisses, intruded by Cretaceous plutons, such as the Asbestos Mountain tonalite. Based on $^{40}Ar/^{39}Ar$ cooling ages on biotite, the gneisses underwent high-temperature plastic deformation between 87 and 65 Ma [*Goodwin and Renne*, 1991]. Multiple sets of pseudotachylyte veins cut through the transition zone between the Asbestos Mountain tonalites and the Palm Canyon gneisses [*Wenk et al.*, 2000; *Rowe et al.*, 2012]. These veins yield a $^{40}Ar/^{39}Ar$ whole-rock plateau age of 59 ± 1 Ma [*Wenk et al.*, 2000]. Temperature in the host rock immediately before pseudotachylyte formation was estimated to 250 to 300°C [*Wenk et al.*, 2000].

The pseudotachylyte samples come from two localities, south of Highway 74 along Deep Canyon and north of Sheep Mountain (Figure 1). In several localities, successive sets of crosscutting pseudotachylyte veins are observed and all of these are hosted by gneisses. The gneisses consist of coarse-grained, ductilely deformed, biotite-hornblende-titanite quartzo-feldspathic assemblages. This gneissic complex also hosts minor bodies of amphibolite, pegmatite and calc-silicate rocks, but no pseudotachylyte veins are observed in these rock types.

The pseudotachylyte veins are roughly parallel to each other, approximately spaced every 10 to 25 m, and strike NW-SE with a NE dip. The sense of coseismic slip, determined at two localities, on the basis of offset macroscopic markers, is top to the southwest. The most continuous veins can be traced over several tens of meters. The thickness of generation veins (see *Grocott* [1981] for a definition) ranges between 2 and 10 mm, depending on locality, but is as thick as 50 mm in pull-apart melt reservoir zones (Figure 2a). Injection veins display a tapered geometry (Figure 2b). Veins are more abundant near or along lithologic boundaries, such as gneiss/pegmatite contacts. Pseudotachylytes also form vein networks that show little preferred orientation of shear fractures. Oxidized pseudotachylyte veins exhibit a surficial maroon color due to formation of iron oxides, while, in contrast, ultracataclasite veins exhibit a light green color. In contrast, unaltered pseudotachylytes appear dark blue to black. The maroon alteration haloes tend to be wider in each vein hanging wall than in their footwall. A dense network of prehnite-chlorite-calcite shear fractures, flanked by maroon alteration haloes, cuts through pseudotachylyte veins, and these exhibit displacements that are less than 2 mm.

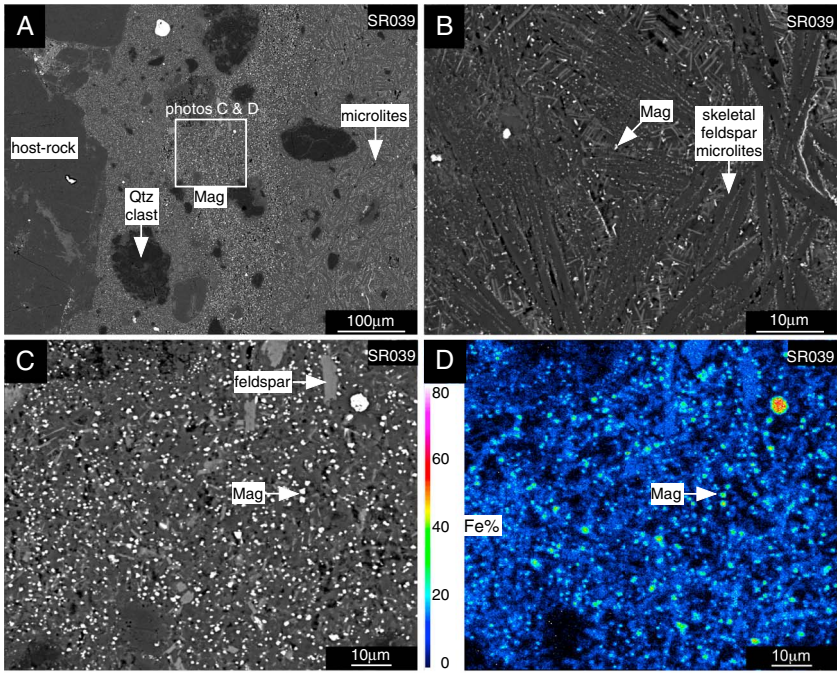


**Figure 3.** Electron microscopy photomicrographs of microstructures of the Santa Rosa pseudotachylyte veins. (a) Sharp contact between zoned pseudotachylyte vein and host rock. Note the corroded quartz clast indicating a high melting temperature. Magnetite grain-rich zones appear in the frame. (b) Detail of a microlite-rich zone resulting in growth of skeletal feldspar crystals attesting of fast quenching. (c) Euhedral, octahedral magnetite grains. (d) Energy dispersive image demonstrating the uniform distribution of iron at a small scale.

## 4. Microstructures of Host Rocks and Pseudotachylyte Veins

### 4.1. Host Rock Microstructures

The Palm Canyon gneisses host the pseudotachylyte veins of this study. These gneisses exhibit a prominent granoblastic to mylonitic foliation that overprints a centimeter-scale metamorphic banding. In a few localities, quartz ribbons of a few tens of millimeters in width and hundreds of millimeters in length attest to localized ultramylonitic deformation. Low-temperature, plastic microstructures, such as mechanical twins in euhedral plagioclase, recrystallized biotite clusters, and undulose extinction in quartz, overprint the high-grade foliation. Near pseudotachylyte veins ($<$20 mm), zircon and plagioclase grains are free of fractures, which indicates moderate differential stress in the damage zone created around the seismic slip plane, i.e., the pseudotachylyte vein. Cataclastic deformation gradually becomes slightly more intense within a millimeter from a pseudotachylyte vein, but the host rock adjacent to veins is not an ultracataclasite. The contact between pseudotachylyte veins and their host rock forms a sharp boundary (Figure 3a) commonly decorated by iron oxides and, in a few places, scattered specular hematite grains up to 7 mm in length [*Ferré et al*., 2005b, 2012].

### 4.2. Pseudotachylyte Microstructures

Our investigations are restricted to those pseudotachylyte veins that bear microstructural evidence for frictional melting, such as thermally corroded quartz grains or skeletal feldspar microlites [*Wenk et al*., 2000; *Ferré et al*., 2005b, 2012]. Both generation veins, parallel to the slip plane, and injection veins, at high angle to the slip plane, exhibit compositional heterogeneity marked by varying modal concentration of magnetite crystals, quartz clasts, and microlites (Figure 3a). The microlites consist mainly of euhedral, calcic plagioclase ranging in size from 5 to 100 µm that locally form radiating microstructures (Figure 3b), although quartz and orthoclase microlites also occur. The large microlites do not display a preferred orientation with respect to vein margin. The size of microlites decreases toward the margins of the vein, particularly in the case of injection veins. The percentage of clasts in all samples examined is less than 40%. These clasts exhibit mechanical twinning in plagioclase, undulose extinction in quartz, and numerous fractures. Quartz grains commonly display a lobate shape. The grain size of these clasts is between about a half and a fifth of the

original grain size in the undeformed host rock. Some of these clasts exhibit corrosion gulfs, concave, and rounded outlines. Ferromagnesian silicates (biotite, hornblende) are very rare in this type of pseudotachylyte. Crystallites (i.e., grains $<5\,\mu m$) form skeletal crystals assembled in a radial pattern similar to volcanic spherulites. The matrix between microlites consists of grains of a refringence higher than feldspar, such as biotite and a calcic amphibole. Magnetite grains in the matrix are subrounded and range in size from 0.2 to 1.0 μm. Their grain size remains relatively constant within broadly defined domains of a few tens of microns in width that parallel the vein margins. These domains represent a primary, flow-related, zonation (Figures 3c and 3d).

## 5. Methods

### 5.1. Field Sampling and Laboratory Preparation

Large oriented samples (2–3 kg) were collected in the field and cut into serial slabs in the laboratory. All slabs are perpendicular to the main pseudotachylyte generation vein. All cuts were made using nonmagnetic diamond saw blades. Thick slabs, 20 mm, were cut for surface mapping of magnetic susceptibility. Additional slabs of a thickness equal to that of the vein, 5 to 10 mm, were prepared for paleomagnetic experiments. Cube-shaped specimens were produced by cutting these thin slabs in the directions along and across the vein using a diamond wire saw. This aspect of our sample preparation is crucial to our study because paleomagnetic specimens should preferably be small enough to consist of pseudotachylyte material only. Scanning electron imagery was performed on a Hitachi S570 microscope at Southern Illinois University.

### 5.2. Rock Magnetism Measurements

Magnetic susceptibility was measured (1) in low field ($K_{lf}$), 0.37 mT, using a Kappabridge KLY-4S susceptometer at 875 Hz for cubes; (2) in low field, 0.25 mT, using a MS2F probe attached to a Bartington MS2 susceptometer at 580 Hz, for magnetic susceptibility mapping; and (3) in high field ($K_{hf}$), up to 1.5 T in direct current, using a Princeton Measurements Micromag vibrating sample magnetometer (VSM) 3900–04 on discrete specimens. The maps of magnetic susceptibility used a square grid at a regular spacing of 1 to 3 mm depending on vein width. The Bartington MS2F probe averages $K_{lf}$ over a half-sphere volume so that the contribution at a depth of 6 mm beneath the probe center is only 10%. Measurements less than 10 mm from the slab edge were discarded. The variation of magnetic susceptibility as a function of temperature was investigated using a CS3 furnace attached to Kappabridge KLY-3S operating at 875 Hz and a field of 0.37 mT, up to 670°C, under argon flux to limit oxidation.

### 5.3. Hysteresis Measurements

The magnetic hysteresis parameters of small specimens ($<4$ g) were measured using a Princeton Measurements vibrating sample magnetometer (VSM) Micromag 3900–04, sensitivity $5{\cdot}10^{-9}$ $Am^2$, up to an applied direct field of 1.5 T. The high-field magnetic susceptibility ($K_{hf}$) was determined above the saturation field ($H_s$) following the approach of *Belley et al*. [2009]. The independent measurement of $K_{lf}$ and $K_{hf}$ allows the calculation of the percentage of paramagnetic susceptibility [*Martín-Hernández and Ferré*, 2007].

### 5.4. First-Order Reversal Curve Analysis

First-Order Reversal Curve (FORC) analysis provides valuable information on the magnetic grain size distribution of ferromagnetic (in a broad sense) grains [e.g., *Pike et al*., 1999; *Roberts et al*., 2000]. FORC analysis assists in the evaluation of magnetic coercivity and magnetic remanence among grains of differing domain states: superparamagnetic (SP), single domain (SD), pseudo-single domain (PSD), or multidomain (MD). The specimen is magnetized to saturation in a high positive field before the field is reduced stepwise and returned to positive saturation after each step. A partial hysteresis loop is produced for each field step and is referred to as a FORC. The set of FORCs is combined to produce the FORC diagram by differentiating $M$ with respect to both fields (reversal field and measurement field) and plotting this quantity in a coordinate system defined by coercive field $H_c$ and bias field $H_u$. SD grains, with high $H_c$ values, contribute to more widely spaced FORCs and appear to the right on FORC diagrams, while MD grains plot near the ordinate and PSD grains plot in between. Asymmetries about the abscissa are due primarily to magnetostatic interactions and accessorily to magnetic viscosity. This asymmetry and the vertical spread of the distribution allow determining the degree, if any, of magnetic grain interactions as an interacting population of magnetic grains. The asymmetry will shift the FORC diagram to positive $H_u$ values and produce a wider $H_u$ axis peak [*Pike et al*., 1999]. FORC measurements were obtained using 100 curves on the VSM, with a field spacing of 5 mT and a positive saturation field of 0.5 T.

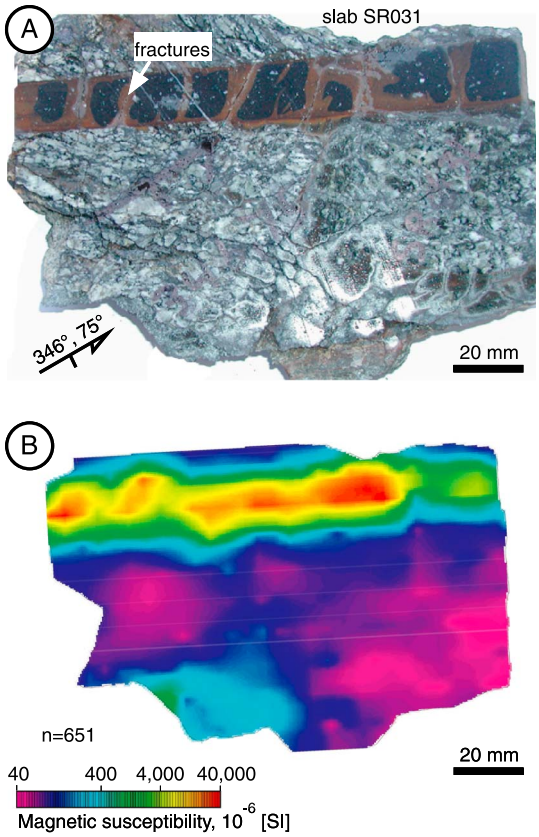


**Figure 4.** (a) Slab sample cut across a pseudotachylyte generation vein. (b) Magnetic susceptibility ($K$) map the same sample showing a significant increase of $K$ between the host rock and the vein, a symmetric zonation of $K$ in the vein, and a pattern of $K$ variations reflecting late fractures along which alteration by meteoric fluids took place long after seismic slip.

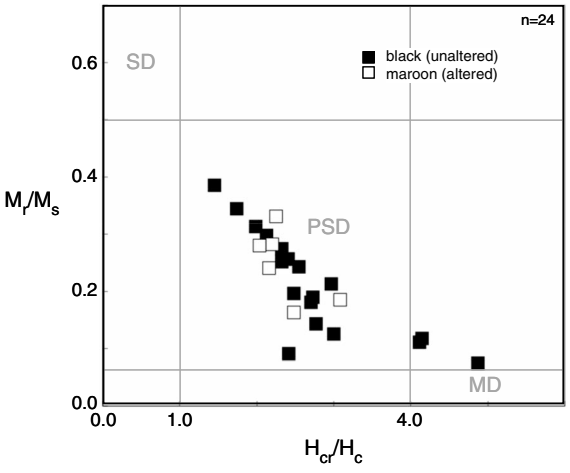


**Figure 5.** $M_r/M_s$ versus $H_{cr}/H_c$ diagram [*Day et al.*, 1977] for small fragments of pseudotachylytes (<3 g). Samples span along a mixing trend between SD and MD, plotting mostly in the PSD domain. The maroon, hematite-bearing specimens are statistically indistinguishable from the black, hematite-free specimens where magnetite dominates the magnetic hysteresis properties.

A smoothing factor of 6 was used, and data were processed and plotted using FORCinel [*Harrison and Feinberg*, 2008]. Plots have been made using the "relaxed-fit" approach [*Muxworthy and Roberts*, 2007].

### 5.5. Demagnetization Experiments

Two complementary sets of stepwise NRM demagnetization (thermal and microwave) experiments were performed on selected specimens. Thermal demagnetization measurements were performed using an ASC TD-48 thermal demagnetization instrument, and remanence measurements were made using a 2G Enterprises 760R three-axes DC superconducting rock magnetometer with a sensitivity of ~$5{\cdot}10^{-11}$ $Am^2$ at the Paleomagnetism Laboratory, University of New Mexico, and at Centre Européen de Recherche et d'Enseignement de Géosciences de l'Environnement, France. Demagnetization results are presented as normalized magnetization intensity decay plots and as orthogonal demagnetization diagrams [*Zijderveld*, 1967]. Microwave demagnetization experiments were performed, as this method has the advantage of producing less heating-induced reactions [e.g., *Walton et al.*, 1993; *Hill and Shaw*, 2000] using the 14 GHz microwave system at the Geomagnetism Laboratory, University of Liverpool [*Shaw*, 2007].

## 6. Results

### 6.1. Spatial Variations of Magnetic Susceptibility of Host Rock and Pseudotachylyte Vein

The magnetic susceptibility ($K_{lf}$) of a representative slab of host rock cut by a pseudotachylyte generation vein was mapped (Figure 4). In the host rock, $K_{lf}$ ranges between 40 and $200{\cdot}10^{-6}$ [SI], with an average of $80{\cdot}10^{-6}$ [SI]. $K_{lf}$ is relatively consistent on the scale of a few $cm^2$ but increases abruptly toward the vein margin. In contrast, in the pseudotachylyte vein, $K_{lf}$ displays a much greater variation between $1100{\cdot}10^{-6}$ and $50{,}000{\cdot}10^{-6}$ [SI], with an average of $11{,}000{\cdot}10^{-6}$ [SI]. Within the pseudotachylyte vein $K_{lf}$ displays a symmetric zonation characterized by higher values in the center than at the margins. This $K_{lf}$ zonation cannot be attributed to an insufficient spatial resolution of the probe because, in other areas of the slab, the same probe revealed

**Table 1.** Magnetic Hysteresis Properties of the Santa Rosa Pseudotachylytes[a]

| SampleUnits | Color | Mass(g) | $M_s$(Am$^2$/kg) | C(%) | $M_r$(Am$^2$/kg) | $H_c$(kA/m) | $H_{cr}$(kA/m) | $H_{cr}/H_c$ | $M_r/M_s$ | $K_{hf}$(10-6 [SI]) | $K_{lf}$(10-6 [SI]) | %para |
|---|---|---|---|---|---|---|---|---|---|---|---|---|
| 001A | black | 0.120 | 3.37 | 3.7 | 1.16 | 30.9 | 53.7 | 1.74 | 0.34 | 2,198 | 77,287 | 2.8 |
| 001B | black | 0.213 | 2.57 | 2.8 | 0.62 | 20.9 | 53.3 | 2.55 | 0.24 | 1,268 | 40,635 | 3.1 |
| 001C | black | 0.093 | 2.57 | 2.8 | 0.23 | 6.4 | 15.5 | 2.41 | 0.09 | 584 | 85,231 | 0.7 |
| 002A | black | 0.130 | 1.52 | 1.6 | 0.39 | 20.6 | 49.5 | 2.40 | 0.26 | 622 | 39,162 | 1.6 |
| 002B | black | 0.242 | 1.92 | 2.1 | 0.41 | 19.0 | 56.3 | 2.96 | 0.21 | 808 | 48,708 | 1.7 |
| 003A | black | 0.120 | 2.02 | 2.2 | 0.60 | 23.6 | 50.2 | 2.13 | 0.30 | 763 | 53,237 | 1.4 |
| 003B | maroon | 0.054 | 1.80 | 2.0 | 0.60 | 27.4 | 61.7 | 2.25 | 0.33 | 905 | 48,624 | 1.9 |
| 004A | black | 0.544 | 3.57 | 3.9 | 0.65 | 14.2 | 38.4 | 2.70 | 0.18 | 1,102 | 99,445 | 1.1 |
| 004B | black | 0.550 | 3.98 | 4.3 | 0.78 | 14.8 | 36.7 | 2.48 | 0.20 | 1,429 | 112,155 | 1.3 |
| 004C | black | 0.368 | 3.61 | 3.9 | 0.69 | 15.3 | 41.8 | 2.73 | 0.19 | 858 | 98,841 | 0.9 |
| 004hemA | maroon | 0.116 | 1.79 | 1.9 | 0.29 | 13.5 | 33.5 | 2.48 | 0.16 | 617 | 52,134 | 1.2 |
| 004hemB | silver-maroon | 0.054 | 1.56 | 1.7 | 0.29 | 12.9 | 39.8 | 3.09 | 0.19 | 505 | 44,716 | 1.1 |
| 005A | black | 0.229 | 0.93 | 1.0 | 0.12 | 11.1 | 33.3 | 3.00 | 0.13 | 330 | 29,434 | 1.1 |
| 005B | black | 0.067 | 2.75 | 3.0 | 0.39 | 11.7 | 32.4 | 2.77 | 0.14 | 733 | 87,965 | 0.8 |
| 006A | maroon | 0.284 | 1.79 | 1.9 | 0.50 | 19.4 | 39.5 | 2.04 | 0.28 | 839 | 51,416 | 1.6 |
| 006B | black | 0.092 | 1.72 | 1.9 | 0.54 | 26.8 | 53.2 | 1.99 | 0.31 | 1,057 | 47,663 | 2.2 |
| 007A | black | 0.207 | 3.07 | 3.3 | 0.34 | 12.1 | 49.8 | 4.12 | 0.11 | 656 | 75,322 | 0.9 |
| 007B | black | 0.209 | 3.67 | 4.0 | 0.28 | 8.0 | 39.0 | 4.87 | 0.07 | 743 | 97,540 | 0.8 |
| 008A | black | 0.170 | 9.59 | 10.4 | 3.70 | 38.7 | 56.1 | 1.45 | 0.39 | 7,751 | 181,621 | 4.3 |
| 008B | black | 0.112 | 6.73 | 7.3 | 0.79 | 11.9 | 49.3 | 4.14 | 0.12 | 1,755 | 172,491 | 1.0 |
| 008C | black | 0.280 | 10.14 | 11.0 | 2.56 | 23.4 | 54.3 | 2.32 | 0.25 | 4,658 | 244,651 | 1.9 |
| 009A | black | 1.786 | 0.63 | 0.7 | 0.18 | 21.6 | 47.5 | 2.20 | 0.28 | 340 | 15,982 | 2.1 |
| 009B | maroon | 3.368 | 1.53 | 1.7 | 0.37 | 17.4 | 37.6 | 2.16 | 0.24 | 709 | 42,768 | 1.7 |
| 010A | black | 0.203 | 1.02 | 1.1 | 0.28 | 23.0 | 53.4 | 2.32 | 0.28 | 821 | 27,144 | 3.0 |
| 011A | black | 0.240 | 4.18 | 4.5 | 0.69 | 22.4 | 48.9 | 2.18 | 0.16 | 1,245 | 46,888 | 2.7 |
| 011B | black | 0.211 | 4.23 | 4.6 | 0.96 | 27.0 | 47.6 | 1.76 | 0.23 | 1,008 | 43,207 | 2.3 |
| 011C | black | 0.259 | 4.12 | 4.5 | 0.44 | 12.2 | 44.6 | 3.66 | 0.11 | 935 | 48,224 | 1.9 |
| 011D | black | 0.200 | 5.38 | 5.8 | 0.59 | 13.4 | 46.6 | 3.48 | 0.11 | 922 | 42,504 | 2.2 |
| 011E | black | 0.212 | 4.64 | 5.0 | 1.03 | 25.7 | 48.9 | 1.90 | 0.22 | 1,056 | 43,009 | 2.5 |
| 011 F | black | 0.233 | 4.38 | 4.8 | 0.63 | 24.2 | 50.1 | 2.07 | 0.14 | 1,261 | 46,995 | 2.7 |
| | *min* | *0.054* | *0.63* | *0.69* | *0.12* | *6.4* | *15.5* | *1.45* | *0.07* | *330* | *15,982* | *0.7* |
| | *max* | *3.368* | *10.14* | *11.02* | *3.70* | *38.7* | *61.7* | *4.87* | *0.39* | *7,751* | *244,651* | *4.3* |
| | *average* | | *3.36* | *3.65* | *0.70* | *19.0* | *45.4* | *2.61* | *0.21* | *1,283* | *71,500* | *1.8* |
| | *SD* | | *2.27* | *2.47* | *0.72* | *7.4* | *9.5* | *0.78* | *0.08* | *1,451* | *50,501* | *0.9* |

[a]Italic style is used to distinguish data for samples from statistical data.

much smaller variations of $K_{lf}$ that are most likely caused by fractures (Figure 4a). The systematic $K_{lf}$ decrease along fractures that postdate pseudotachylyte formation must reflect a significant variation in abundance and/or nature of ferromagnetic minerals in the vein.

### 6.2. Magnetic Hysteresis Properties and FORC Analysis

The Santa Rosa pseudotachylytes generally reach magnetic saturation at a field between 100 and 700 mT, with a median saturation field for unaltered specimens of about 250 mT [*Ferré et al*., 2005b, 2012]. This relatively low saturation field, combined with the Curie temperatures determined through thermomagnetic experiment, is consistent with magnetite as the main ferromagnetic phase. Further, the magnetic hysteresis properties of the pseudotachylytes indicate grain sizes in the pseudo-single-domain (PSD) range, although a few specimens plot near the multidomain (MD) field (Figure 5). Oxidized pseudotachylytes display hysteresis properties similar to those of the unaltered veins. The high-field magnetic susceptibility ($K_{hf}$) of the pseudotachylytes ranges from $330{\cdot}10^{-6}$ to $7751{\cdot}10^{-6}$ [SI] with an average of $1283{\cdot}10^{-6}$ [SI] (Table 1). The percentage of paramagnetic susceptibility in the pseudotachylyte ranges from 0.7 to 4.3% but remains generally low with an average of 1.8%. FORC measurements provide additional information on the distribution of magnetic coercivities along a transect through a representative pseudotachylyte vein (Figure 6). The proportion of interacting SD grains is lower near the center of the vein (specimen SR011D) and increases toward the margins (specimens SR011A and SR011F). The marginal zones of the vein also display a greater proportion of MD grains (specimens SR011A and SR011F) and a wider distribution of grain sizes. Overall, unaltered pseudotachylyte veins typically host a mixture of MD and PSD magnetite grains and no hematite.

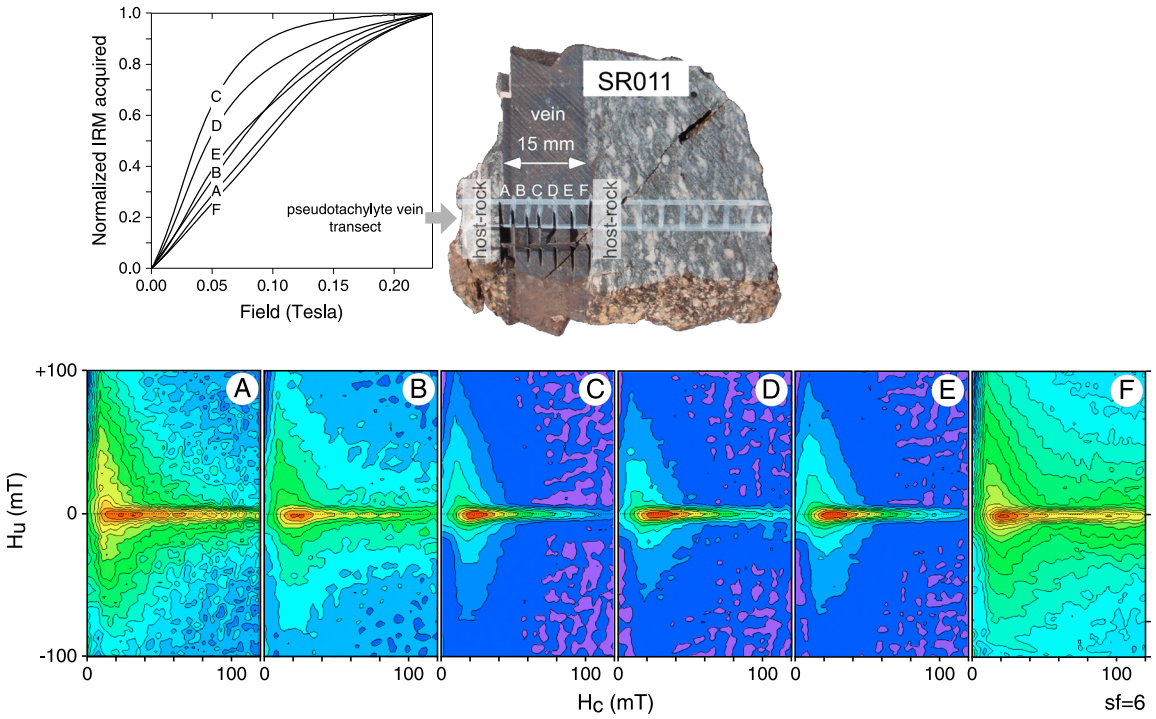


**Figure 6.** First-order reversal curve (FORC) diagrams from (a–f) six pseudotachylyte specimens cut along a transect across a vein. Figure 6d shows a lower proportion of interacting SD grains, while this proportion increases toward the margins shown in Figures 6a and 6f. The normalized IRM acquired (inset) shows magnetically harder grains toward the margins. See text for analytical details.

### 6.3. Thermomagnetic Experiments

The magnetic susceptibility ($K_{lf}$) of oxidized and unaltered pseudotachylytes, SR031A and SR031B respectively, shows a characteristic ferromagnetic behavior with an abrupt drop at a Curie temperature of about 578°C (Figure 7), implying very low Ti magnetite as the main magnetic phase present. The nonreversible behavior exhibited in thermomagnetic experiments demonstrates that the original magnetic assemblage is unstable at elevated temperature, possibly because a fine magnetite granulometry promotes oxidation upon heating. The magnetic susceptibility ($K_{lf}$) measured between progressive thermal demagnetization steps (Figure 8) reveals a behavior similar to that shown in Figure 7, with fresh pseudotachylyte displaying thermal stability up to about 325°C. The magnetic susceptibility of oxidized pseudotachylyte, on the other hand, changes above 80°C.

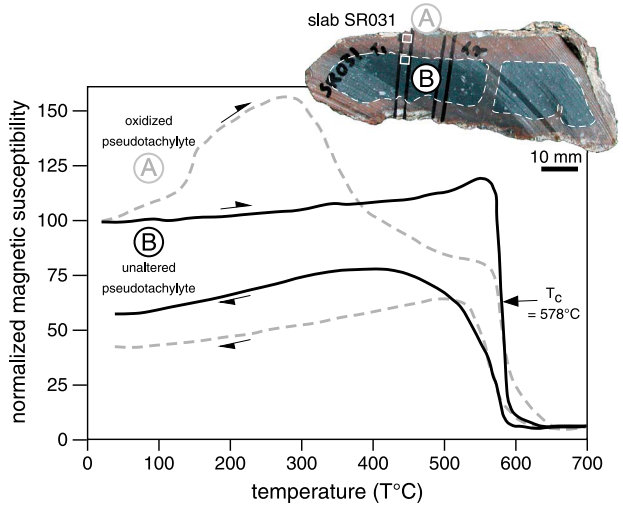


**Figure 7.** Bulk susceptibility versus temperature experiments on unaltered (dash line) and oxidized (solid line) pseudotachylytes from the same slab. The unaltered pseudotachylyte shows the characteristic behavior of stoichiometric magnetite (Curie temperature = 578°C). The oxidized pseudotachylyte shows a nonreversible behavior characterized by the persistence of a small contribution to magnetic susceptibility above 600°C, attributed to hematite, and a low stability at low temperature.

### 6.4. Isothermal Remanent Magnetization Acquisition Curves

Isothermal Remanent Magnetization (IRM) acquisition curves of specimens from a traverse across a pseudotachylyte vein display contrasting approaches to magnetic saturation depending on their

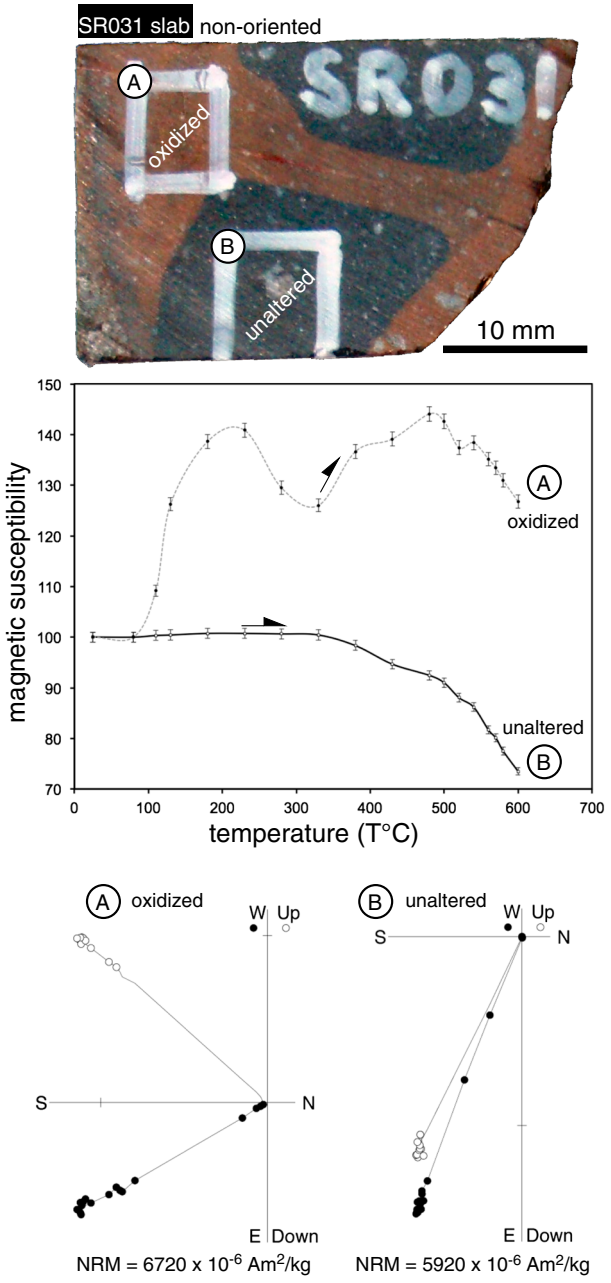


**Figure 8.** Stepwise thermal demagnetization of NRM of an (a) oxidized and (b) unaltered pseudotachylyte. The specimens exhibit distinct demagnetization behaviors with the oxidized specimen less mineralogical stability than the unaltered specimen as shown by the discrete magnetic measurements taken after each demagnetization step. Both specimens show stable demagnetizations characterized by one major directional component, but the magnetization directions of the two specimens strongly differ. Data presented in the specimen framework (uncorrected).

position with respect to the vein (Figure 6). Most specimens, including specimens A and F from the margins of the vein, do not saturate with the maximum applied field of 250 mT. The approaches to saturation of specimens A, B, D, E, and F indicate the contribution of magnetically hard phases such as hematite or goethite. In contrast, specimen C, in the central part of the vein, is almost fully saturated by 150 mT, and this is consistent with a magnetic assemblage dominated by a magnetically soft mineral such as PSD-MD magnetite. These results further indicate that the ferromagnetic assemblage across a pseudotachylyte vein is heterogeneous.

### 6.5. Initial Thermal Demagnetization of NRM Experiments

Progressive thermal demagnetization experiments were performed on five cubes (10 mm on a side) cut from two slab samples along pseudotachylyte generation veins in order to assess the general thermal demagnetization behavior and laboratory unblocking temperature spectra of pseudotachylyte. Some specimens reveal a thermally discrete laboratory unblocking temperature spectrum, with unblocking at about 500°C (Figure 9). Specimens SR003A03, SR003A15, and to some extent SR010-03 show a more distributed laboratory unblocking temperature spectra between 200 and 400°C. The NRM intensity of specimens from slab sample SR003A varies by 3 orders of magnitude along the vein, from $4891{\cdot}10^{-6}$ to $1.11{\cdot}10^{-6}$ Am$^2$/kg, whereas the NRM intensity of specimens along slab sample SR010, through a generation vein, is more consistent. The NRM intensity is highest in specimen SR003A03, which shows the highest pseudotachylyte/host rock ratio. Overall, these initial demagnetization experiments document two well-defined magnetization components (Figure 9). The second removed is a relatively high laboratory unblocking temperature component (HT, >300°C), oriented at high angles (65 to 85°) to the vein, while the first removed is a relatively low laboratory unblocking temperature component (LT, < ≈300°C), oriented at low angles (5 to 15°) to the vein.

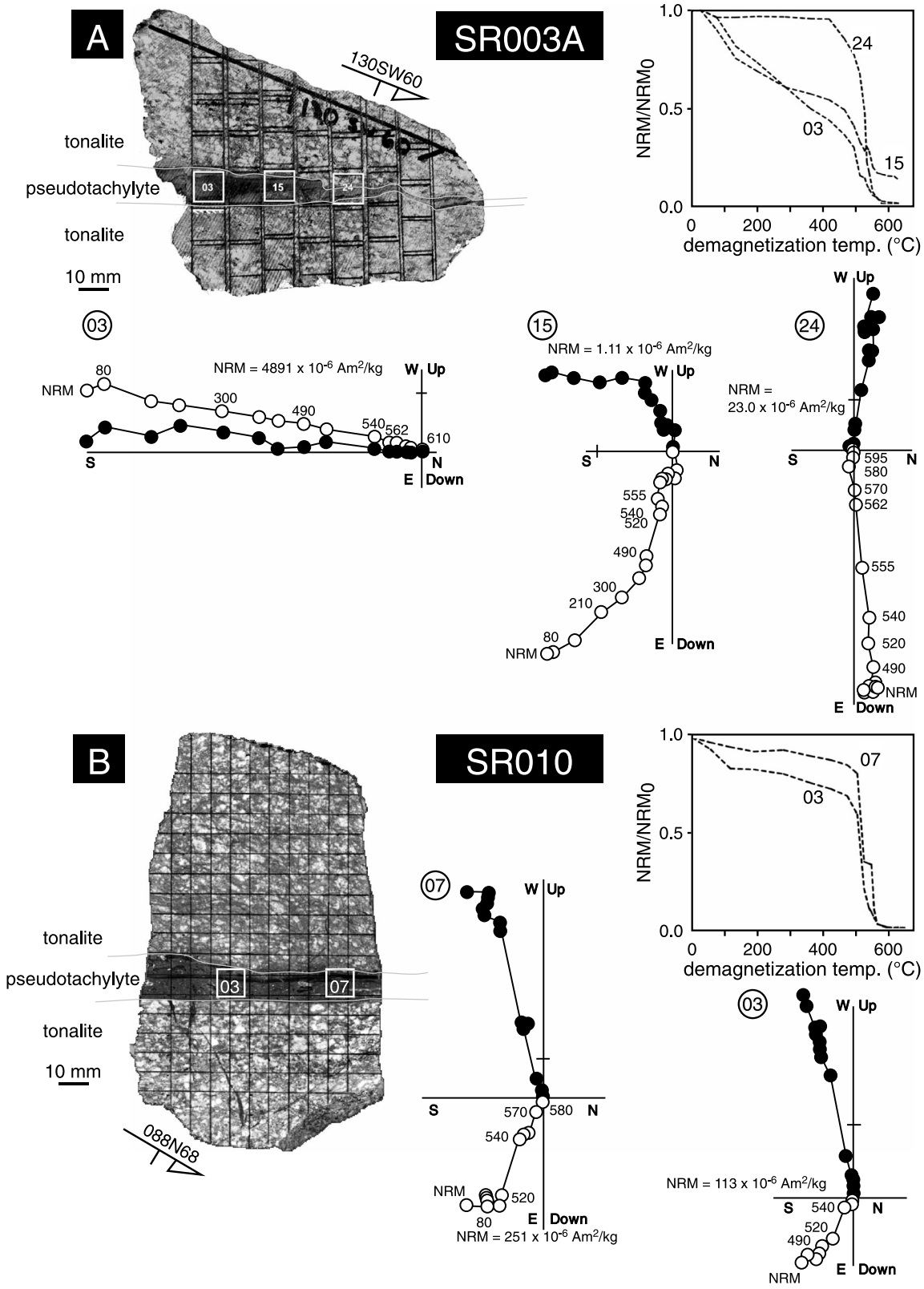


**Figure 9.** Orthogonal diagrams of stepwise NRM demagnetization. Data presented in the specimen framework (uncorrected). (a) Slab SR003A. The three specimens were cut along a pseudotachylyte generation vein and display 2 orders of magnitude difference in magnetization intensities. The three specimens also exhibit different demagnetization directions. (b) Slab SR010. In contrast, the pseudotachylyte specimens from this slab show consistent NRM intensities and directions. Overall, these two slabs document a magnetization process characterized by a high variability in magnetization intensity and direction.

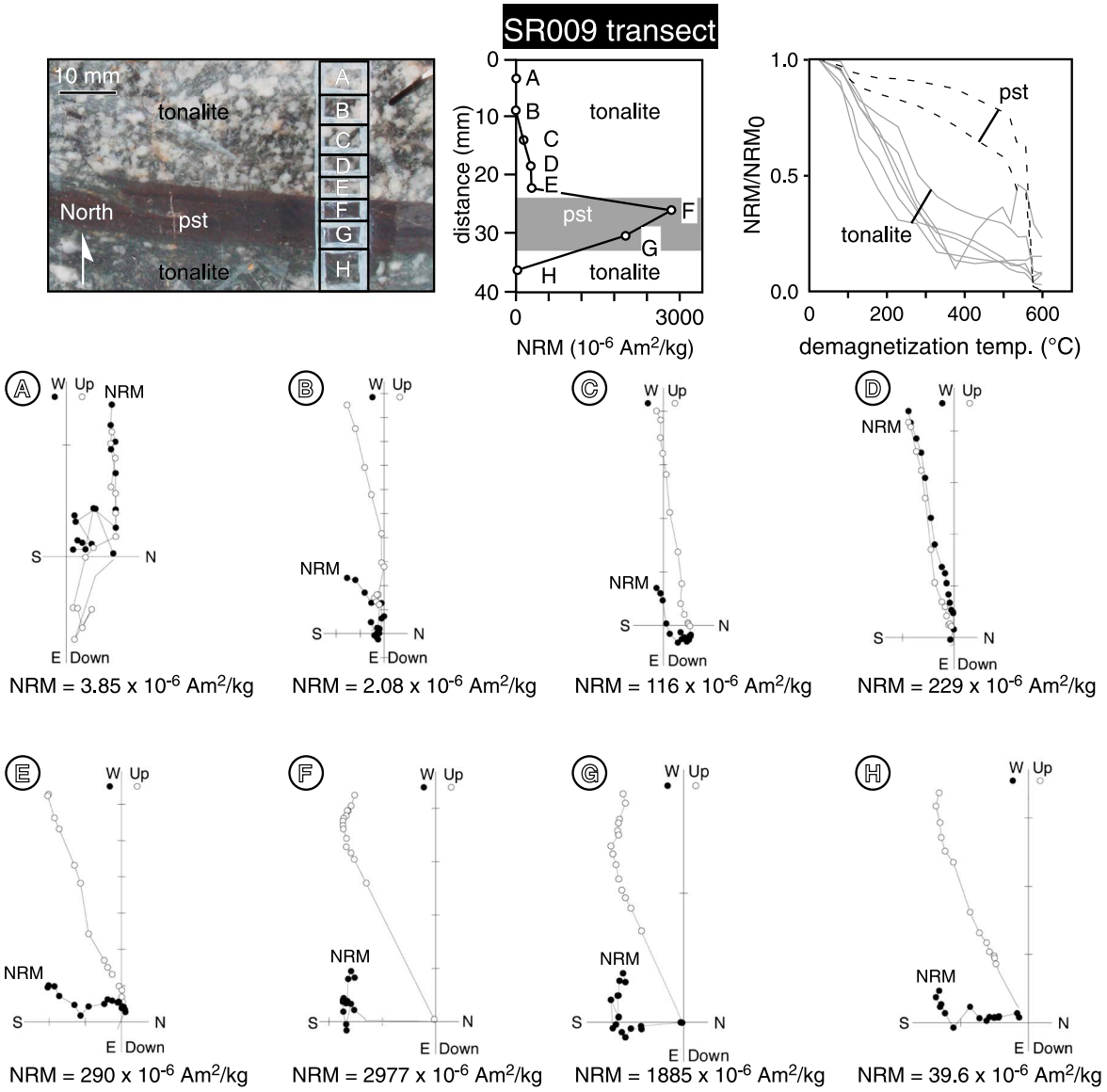


**Figure 10.** Orthogonal diagrams of stepwise NRM demagnetization of pseudotachylyte transect SR009. Data presented in the specimen framework (uncorrected). This transect shows a distinctively higher NRM intensity in the pseudotachylyte vein than in the host rock, as well as two components of demagnetization characterized by a low- and a high- unblocking temperature. The NRM thermal demagnetization experiments also demonstrate that this slab has not been completely remagnetized after seismic slip and preserves an original TRM overprinted by a CRM attributed to meteoric fluid alteration.

### 6.6. Transect Thermal Demagnetization of NRM Experiments

To clarify the origin of the two NRM components identified in the thermal demagnetization experiments and the cause of intensity variations, we performed a series of additional thermal demagnetization experiments on 40 specimens (≈6 × 4 × 2 mm parallelepipeds) cut from transects across three slabs and perpendicular to generation veins (Figures 10–12).

In general, the host rock (tonalite) and the pseudotachylyte display contrasting response to progressive thermal demagnetization. Host rock typically exhibits relatively rapid unblocking from 100 to 550°C, whereas pseudotachylyte retains as much as 50% of the original NRM up to 550°C. The NRM intensity of the host rock is typically below $10{\cdot}10^{-6}$ $Am^2/kg$, while the NRM intensity of the pseudotachylyte ranges widely, from about $20{\cdot}10^{-6}$ to $3000{\cdot}10^{-6}$ $Am^2/kg$. NRM intensities of pseudotachylyte tend to be higher toward vein centers. The host rock NRM intensity increases slightly toward the vein at a distance about equal to the vein thickness.

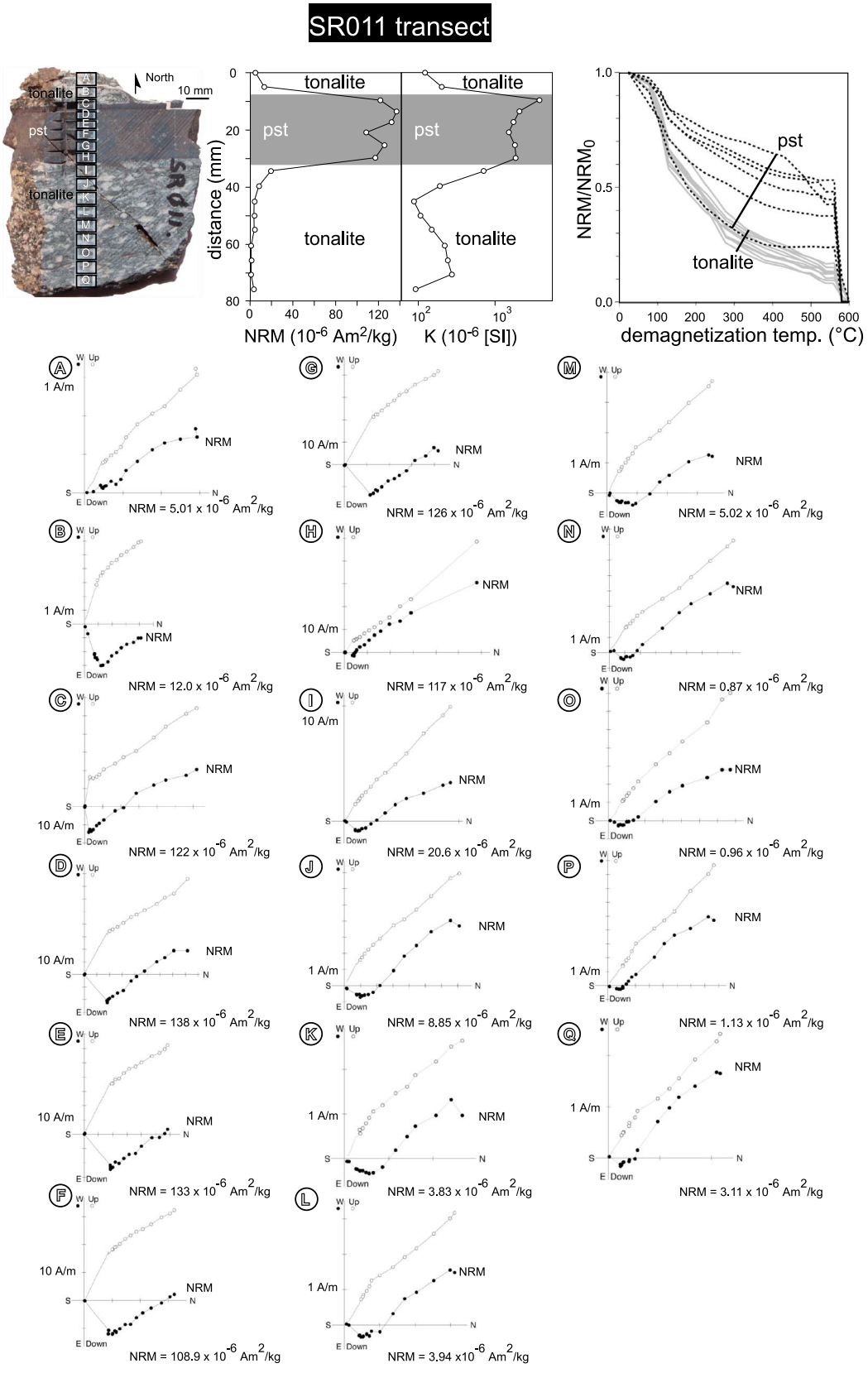


**Figure 11.** Orthogonal diagrams of stepwise NRM demagnetization of pseudotachylyte transect SR011. Same comments as for SR009. Data presented in the specimen framework (uncorrected).

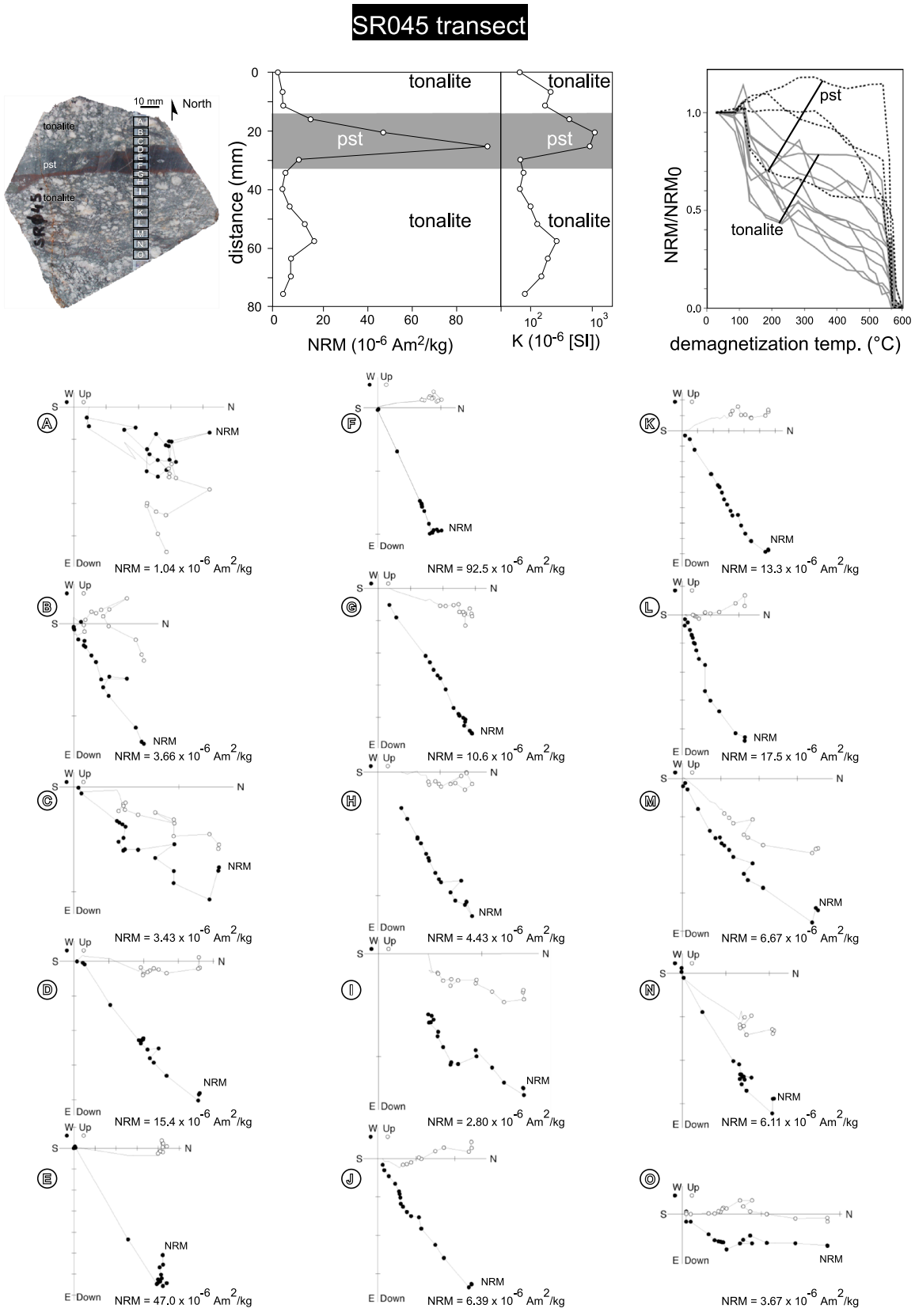


**Figure 12.** Orthogonal diagrams of stepwise NRM demagnetization of pseudotachylyte transect SR045. Same comments as for SR009. Data presented in the specimen framework (uncorrected).

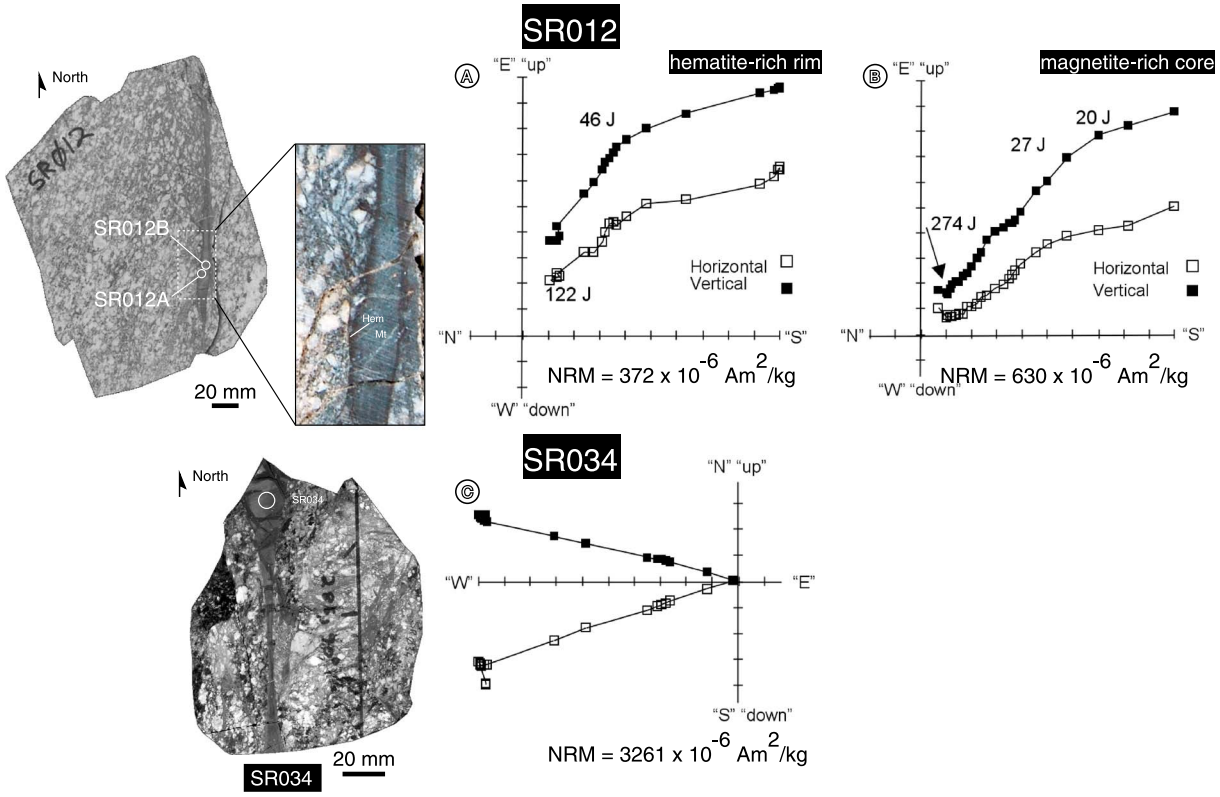


**Figure 13.** Microwave demagnetization of the NRM performed on oxidized (SR012A) and unaltered (SR012B) pseudotachylyte specimens. Data presented in the specimen framework (uncorrected). The microwave approach confirms the results obtained by thermal demagnetization, including the definition of two components comprising the NRM, namely, a low-blocking temperature TRM carried by magnetite and a high-blocking temperature CRM carried by hematite. The two components overlap slightly as indicated by the curved paths of the demagnetization curves.

In slab SR009, the orthogonal demagnetization diagrams reveal two main magnetization components, and these are present in both the host rock and the pseudotachylyte (Figure 10). In host rock specimens over twice vein width from the pseudotachylyte vein, the high laboratory unblocking temperature (HT, >300°C) magnetization component is directionally unstable (SR009A); however, this component becomes better defined in host rock specimens closer to the vein (SR009B to SR009E). In close proximity to the pseudotachylyte vein, host rock specimens SR009E and SR009H display high laboratory unblocking temperature magnetization directions similar to that of the pseudotachylyte vein. In addition to this high laboratory unblocking temperature component, the two pseudotachylyte specimens (SR009F and SR009G) also show a low unblocking temperature (LT, <300°C) magnetization that differs in direction from the high laboratory unblocking temperature component.

In specimens from slab SR011, the orthogonal demagnetization diagrams systematically display two magnetization components, both in the host rock and the pseudotachylyte (Figure 11). The high laboratory unblocking temperature component (MT or HT >300°C) has a higher magnetization intensity in the pseudotachylyte than in the host rock. The directions of this component are different in the host rock and in the pseudotachylyte.

In slab SR045, the orthogonal demagnetization diagrams show two magnetization components in the pseudotachylyte and one component only in the host rock (Figure 12). The direction of the high unblocking temperature magnetization component in the pseudotachylyte is consistent between the two pseudotachylyte specimens (SR045E and SR045F) near the vein center.

### 6.7. Microwave Demagnetization and Paleointensity Experiments

NRM was investigated by microwave demagnetization, up to 300 J. The scalar and vectorial results are comparable to those obtained with thermal demagnetization (Figure 13). The hematite-rich pseudotachylyte specimen SR012-A, located near the margin of a vein, displays two stable NRM components (Figure 13).

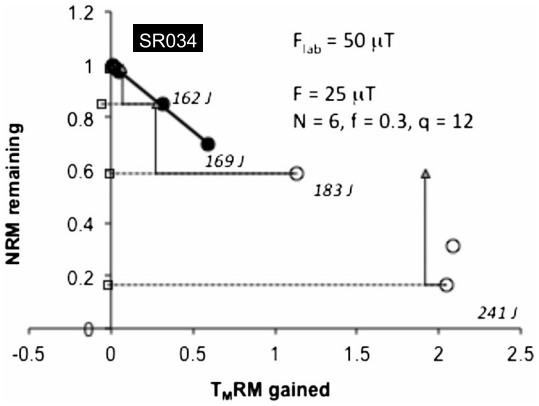


**Figure 14.** Microwave paleointensity experiment on unaltered pseudotachylyte SR034. The intensity of the paleomagnetic field responsible for the TRM of this specimen is estimated to 25 μT.

In contrast, in the magnetite-rich pseudotachylyte specimen SR012-B, one of the two components is more subdued. The specimen SR034-A has the highest NRM and a single-component magnetization.

A microwave paleointensity test was carried out on a pseudotachylyte specimen from SR034. The *Coe* [1967] version of the Thellier method [*Thellier and Thellier*, 1959] was used and incorporated partial microwave thermal remanent magnetization ($pT_MRM$) tail and $pT_MRM$ checks to monitor alteration and multidomain behavior. The resulting NRM/$T_M$RM plot with associated orthogonal vector plot is shown in Figure 14. As with the microwave demagnetization of NRM experiment, the specimen exhibits a single component of magnetization. There is a linear relationship between NRM and $T_MRM$ until 169 J after which linearity breaks down and the checks fail. The behavior is consistent with a remanence of thermal or chemical origin. Basalt samples containing lightning-induced remanence show minimal $T_MRM$ acquisition in comparison to the loss of NRM [e.g., *Hill et al*., 2006, Figure 5]. If the NRM is assumed to be a TRM carried by single-domain magnetite grains, then the strength of the field at the time of remanence acquisition can be estimated to be 25 μT. The magnitude of this magnetic field compares with a low geomagnetic field which also supports the interpretation of the NRM as being primarily a TRM.

Although the microwave paleointensity method, as compared to the more traditional Thellier style methods, tends to minimize mineralogic alteration during the experiment, the breakdown in linearity on the NRM/$T_M$RM plot associated with failing $pT_MRM$ checks indicates that changes to the magnetic mineralogy occurred. An alternative approach for future paleointensity investigations that attempt to circumvent these alteration problems could be to use methods based on alternating field demagnetization, such as the REM′ method [*Gattacceca and Rochette*, 2004].

### 6.8. Directions of Magnetizations Isolated in Progressive Demagnetization in the Pseudotachylyte Vein Structural Framework

The NRM of the coarse-grained tonalitic host rock and of the pseudotachylyte vein generally consists of a low laboratory unblocking temperature component (LT, <300°C) and a high laboratory unblocking temperature component (HT, >300°C). Both LT and HT stable directions of three detailed transects vary substantially between specimens (Table 2 and Figure 15). The pseudotachylyte veins display consistent directions of the LT component. The fact that the pseudotachylyte NRM in samples SR009 and SR010 lies close to the respective pseudotachylyte generation plane suggests that the NRM acquisition might be anisotropic.

## 7. Discussion

The Santa Rosa pseudotachylytes formed in the Palm Canyon Complex gneiss, a biotite-hornblende-titanite quartzo-feldspathic host rock characterized by strong lithologic banding and pervasive mylonitic foliation [*Wenk et al*., 2000; *Ferré et al*., 2012]. Pseudotachylyte generation veins in the sampling area broadly parallel the mylonitic fabric, whereas injection veins and reservoirs tend to be highly oblique to host rock foliation (Figure 2). This observation strongly suggests that the banding and foliation plane strongly controlled seismic slip.

The main carriers of magnetic remanence in the Santa Rosa pseudotachylytes consist of stoichiometric magnetite ($Fe_3O_4$) and hematite ($\alpha$-$Fe_2O_3$) (Figures 3, 4, and 6–8). Magnetite forms mixtures of euhedral PSD and finer grain size fractions, with possible grain size variations near vein margins (Figures 3, 5, and 6). The euhedral shape, locally uniform grain size, and uniform distribution of the magnetite grains (<5 μm; Figure 3) support their nucleation and growth in the pseudotachylyte melt. In addition, the spatial association of

**Table 2.** Thermal Demagnetization Directions of Five Pseudotachylyte Veins and Host Rock[a]

| | | | | Sample | | Geographic | | | |
|---|---|---|---|---|---|---|---|---|---|
| Sample | Temperature Range (°C) | Component | *n* Data | D° | I° | D° | I° | Maximum Angular Deviation (MAD) | Lithology |
| 003A03 | 025–490 | L | 8 | 183 | −10 | 220 | 50 | 5.4 | pseudotachylyte |
| 003A03 | 490–665 | H | 10 | 186 | −14 | 224 | 46 | 2.3 | pseudotachylyte |
| 003A15 | 025–440 | L | 7 | 184 | 42 | 36 | 78 | 5.4 | pseudotachylyte |
| 003A15 | 490–665 | H | 13 | 243 | 61 | 7 | 40 | 9.7 | pseudotachylyte |
| 003A24 | 080–490 | L | 7 | 268 | 37 | 341 | 21 | 27.7 | pseudotachylyte |
| 003A24 | 520–580 | M | 6 | 281 | 61 | 9 | 22 | 1.8 | pseudotachylyte |
| 003A24 | 595–665 | H | 6 | 296 | 70 | 20 | 21 | 16.3 | pseudotachylyte |
| 010-03 | 025–490 | L | 7 | 252 | 14 | 285 | 28 | 8.1 | pseudotachylyte |
| 010-03 | 490–665 | H | 11 | 260 | 18 | 284 | 19 | 3.3 | pseudotachylyte |
| 010-07 | 025–440 | L | 6 | 282 | 22 | 278 | −1 | 19.6 | pseudotachylyte |
| 010-07 | 490–665 | H | 10 | 256 | 30 | 297 | 15 | 1.5 | pseudotachylyte |
| 009A | 025–280 | L | 7 | 268 | −40 | 127 | 2 | 6.5 | host rock |
| 009B | 025–180 | L | 5 | 221 | −71 | 90 | 14 | 3.6 | host rock |
| 009B | 180–600 | H | 13 | 286 | −72 | 94 | −5 | 13.3 | host rock |
| 009C | 025–280 | L | 7 | 288 | −66 | 100 | −7 | 5.3 | host rock |
| 009C | 330–600 | H | 10 | 344 | −80 | 80 | −10 | 11.3 | host rock |
| 009D | 025–600 | H | 17 | 259 | −46 | 121 | 8 | 3.7 | host rock |
| 009E | 025–560 | H | 14 | 194 | −69 | 82 | 20 | 3.5 | host rock |
| 009 F | 025–280 | L | 7 | 244 | −58 | 106 | 13 | 19.3 | pseudotachylyte |
| 009 F | 330–600 | H | 10 | 296 | −2 | 165 | −26 | 6.4 | pseudotachylyte |
| 009G | 025–280 | L | 6 | 245 | −60 | 105 | 12 | 11.4 | pseudotachylyte |
| 009G | 330–600 | H | 9 | 6 | −67 | 75 | −23 | 3.9 | pseudotachylyte |
| 009H | 025–230 | L | 6 | 294 | −63 | 102 | −11 | 9.4 | host rock |
| 009H | 230–600 | H | 11 | 10 | −65 | 72 | −25 | 3.1 | host rock |
| 11A2 | 180–380 | L | 5 | 316 | −38 | 146 | −15 | 4.2 | host rock |
| 11A2 | 430–600 | H | 8 | 337 | −55 | 166 | −26 | 7.5 | host rock |
| 11B2 | 025–430 | L | 10 | 324 | −34 | 151 | −9 | 3.9 | host rock |
| 11B2 | 430–600 | H | 8 | 69 | −47 | 228 | −31 | 3.7 | host rock |
| 11C2 | 180–540 | M | 10 | 322 | −26 | 146 | −2 | 4.0 | pseudotachylyte |
| 11C2 | 560–600 | H | 3 | 80 | −48 | 234 | −36 | 0.6 | pseudotachylyte |
| 11D2 | 080–560 | M | 14 | 322 | −26 | 146 | −2 | 2.0 | pseudotachylyte |
| 11D2 | 560–600 | H | 3 | 50 | −50 | 214 | −27 | 1.0 | pseudotachylyte |
| 11E2 | 130–560 | M | 11 | 324 | −30 | 149 | −5 | 4.2 | pseudotachylyte |
| 11E2 | 560–600 | H | 3 | 51 | −52 | 213 | −29 | 0.8 | pseudotachylyte |
| 11 F2 | 110–540 | M | 11 | 328 | −30 | 153 | −4 | 3.2 | pseudotachylyte |
| 11 F2 | 560–600 | H | 3 | 51 | −52 | 213 | −29 | 0.2 | pseudotachylyte |
| 11G2 | 180–560 | M | 11 | 326 | −34 | 152 | −8 | 2.6 | pseudotachylyte |
| 11G2 | 560–600 | H | 3 | 49 | −49 | 213 | −26 | 0.8 | pseudotachylyte |
| 11H2 | 230–560 | M | 10 | 317 | −27 | 143 | −4 | 4.6 | pseudotachylyte |
| 11H2 | 560–600 | H | 3 | 22 | −53 | 194 | −24 | 2.0 | pseudotachylyte |
| 11I2 | 180–520 | M | 9 | 325 | −39 | 153 | −13 | 4.0 | host rock |
| 11I2 | 560–600 | H | 3 | 40 | −50 | 207 | −25 | 3.7 | host rock |
| 11 J2 | 080–330 | L | 7 | 316 | −31 | 143 | −8 | 3.9 | host rock |
| 11 J2 | 330–560 | M | 8 | 353 | −50 | 175 | −20 | 7.6 | host rock |
| 11 J2 | 560–600 | H | 3 | 31 | −57 | 199 | −30 | 1.0 | host rock |
| 11 K2 | 080–330 | L | 7 | 316 | −31 | 143 | −8 | 3.8 | host rock |
| 11 K2 | 330–560 | M | 8 | 14 | −56 | 189 | −27 | 5.1 | host rock |
| 11 K2 | 560–600 | H | 3 | 43 | −59 | 205 | −34 | 3.9 | host rock |
| 11 L2 | 080–280 | L | 6 | 320 | −32 | 147 | −8 | 5.9 | host rock |
| 11 L2 | 280–560 | M | 9 | 347 | −55 | 172 | −26 | 8.1 | host rock |
| 11 L2 | 560–600 | H | 3 | 41 | −49 | 208 | −24 | 4.0 | host rock |
| 11 M2 | 080–280 | L | 6 | 325 | −35 | 152 | −9 | 4.6 | host rock |
| 11 M2 | 280–560 | M | 9 | 10 | −55 | 186 | −25 | 4.0 | host rock |
| 11 M2 | 560–600 | H | 3 | 40 | −60 | 203 | −34 | 8.2 | host rock |
| 11 N2 | 180–430 | L | 6 | 318 | −28 | 144 | −5 | 2.1 | host rock |
| 11 N2 | 430–560 | M | 6 | 350 | −53 | 174 | −23 | 9.0 | host rock |
| 11 N2 | 560–600 | H | 3 | 37 | −48 | 206 | −22 | 7.6 | host rock |
| 11O2 | 080–330 | L | 7 | 331 | −39 | 157 | −12 | 4.4 | host rock |
| 11O2 | 330–560 | M | 8 | 339 | −51 | 166 | −22 | 5.2 | host rock |
| 11O2 | 560–600 | H | 3 | 29 | −50 | 200 | −23 | 5.8 | host rock |

**Table 2.** (continued)

| Sample | Temperature Range (°C) | Component | *n* Data | Sample D° | Sample I° | Geographic D° | Geographic I° | Maximum Angular Deviation (MAD) | Lithology |
|---|---|---|---|---|---|---|---|---|---|
| 11P2 | 500–580 | H | 5 | 355 | −49 | 177 | −19 | 8.8 | host rock |
| 11P2 | 130–500 | M | 8 | 315 | −37 | 144 | −14 | 2.8 | host rock |
| 11P2 | 560–600 | H | 3 | 15 | −53 | 190 | −24 | 2.2 | host rock |
| 11Q2 | 330–560 | M | 8 | 334 | −52 | 163 | −24 | 6.3 | host rock |
| 11Q2 | 130–330 | L | 5 | 306 | −26 | 133 | −7 | 3.8 | host rock |
| 11Q2 | 560–600 | H | 3 | 35 | −51 | 203 | −25 | 1.3 | host rock |
| 45AT | 025–600 | H | 17 | 32 | 55 | - | - | 25.7 | host rock |
| 45BT | 025–330 | L | 7 | 58 | 31 | - | - | 7.0 | host rock |
| 45BT | 380–540 | M | 6 | 55 | −42 | - | - | 12.5 | host rock |
| 45BT | 560–600 | H | 4 | 115 | 75 | - | - | 33.5 | host rock |
| 45CT | 110–600 | H | 16 | 40 | 17 | - | - | 12.6 | host rock |
| 45DT | 130–570 | M | 13 | 54 | 8 | - | - | 6.9 | pseudotachylyte |
| 45DT | 570–600 | H | 3 | 19 | −35 | - | - | 13.0 | pseudotachylyte |
| 45ET | 025–540 | M | 15 | 276 | −17 | - | - | 22.6 | pseudotachylyte |
| 45ET | 540–600 | H | 5 | 59 | 3 | - | - | 1.1 | pseudotachylyte |
| 45FT | 330–600 | H | 11 | 246 | 4 | - | - | 1.1 | pseudotachylyte |
| 45GT | 180–600 | H | 12 | 58 | 10 | - | - | 2.4 | pseudotachylyte |
| 45HT | 180–600 | H | 13 | 61 | 8 | - | - | 5.7 | host rock |
| 45IT | 110–280 | L | 5 | 42 | 18 | - | - | 9.1 | host rock |
| 45IT | 330–580 | H | 10 | 64 | 13 | - | - | 8.3 | host rock |
| 45JT | 130–520 | M | 9 | 53 | −15 | - | - | 3.8 | host rock |
| 45JT | 520–600 | H | 6 | 58 | 15 | - | - | 4.2 | host rock |
| 45KT | 130–560 | M | 10 | 60 | −2 | - | - | 4.0 | host rock |
| 45KT | 560–600 | H | 4 | 57 | −15 | - | - | 2.7 | host rock |
| 45LT | 080–230 | L | 5 | 50 | −16 | - | - | 7.0 | host rock |
| 45LT | 330–600 | H | 11 | 70 | 4 | - | - | 6.5 | host rock |
| 45MT | 110–230 | L | 5 | 35 | 11 | - | - | 4.7 | host rock |
| 45MT | 330–600 | H | 11 | 56 | 26 | - | - | 4.3 | host rock |
| 45NT | 130–600 | H | 13 | 61 | 23 | - | - | 3.3 | host rock |
| 45OT | 080–380 | L | 6 | 360 | 9 | - | - | 7.5 | host rock |
| 45OT | 430–600 | H | 9 | 36 | −4 | - | - | 8.2 | host rock |

[a]SR045 is a nonoriented float (directions given in specimen reference framework).

euhedral magnetite grains with skeletal feldspar microlites constitutes further evidence that both types of grains formed during quenching of the silicate melt and not through slow devitrification as described elsewhere [*Maddock*, 1983; *Techmer et al*., 1992, 1996].

The host rock is characterized by coarser magnetite grains of significantly larger size (>50 μm) [*Wenk et al*., 2000; *Ferré et al*., 2012]. The pseudotachylyte grains share remarkable morphological and size similarities with grains formed in artificial pseudotachylytes [*Nakamura et al*., 2002]. The relicts of partially molten mafic silicates in some pseudotachylyte veins further suggest that magnetite formed primarily through breakdown of biotite and titanite, as temperature increased during seismic slip [*Ferré et al*., 2012]. Because frictional melting in fault pseudotachylytes results directly from earthquakes, magnetite grains must grow after the beginning of seismic slip and before quenching of the remaining melt documented by the glassy to amorphous matrix that surrounds microlites.

Hematite forms reddish grains disseminated throughout the oxidized rims of pseudotachylytes [*Ferré et al*., 2012] (Figure 7). Generation veins and injection veins are generally altered through a similar thickness of material, suggesting that alteration took place after seismic slip and not through pressurized seismic fluids. The observation that the upper part of a vein usually shows a thicker weathering rind than the lower part hints that meteoric fluids caused this alteration. Also, the pattern of alteration of pseudotachylyte veins follows that of relatively recent calcite fractures (Figure 4), which indicates that this alteration most likely occurred during exhumation of the Palm Canyon Complex. Considering the magnetic data presented here, we cannot exclude the presence of small amounts of maghemite ($\gamma$-$Fe_2O_3$) or goethite (FeO(OH)), two commonly reported ferromagnetic in a broad sense phases in pseudotachylytes [*Nakamura and Nagahama*, 2001; *Fukuchi*, 2003; *Ferré et al*., 2005a; *Hirono et al*., 2006; *Zechmeister et al*., 2007; *Molina Garza et al*., 2009].

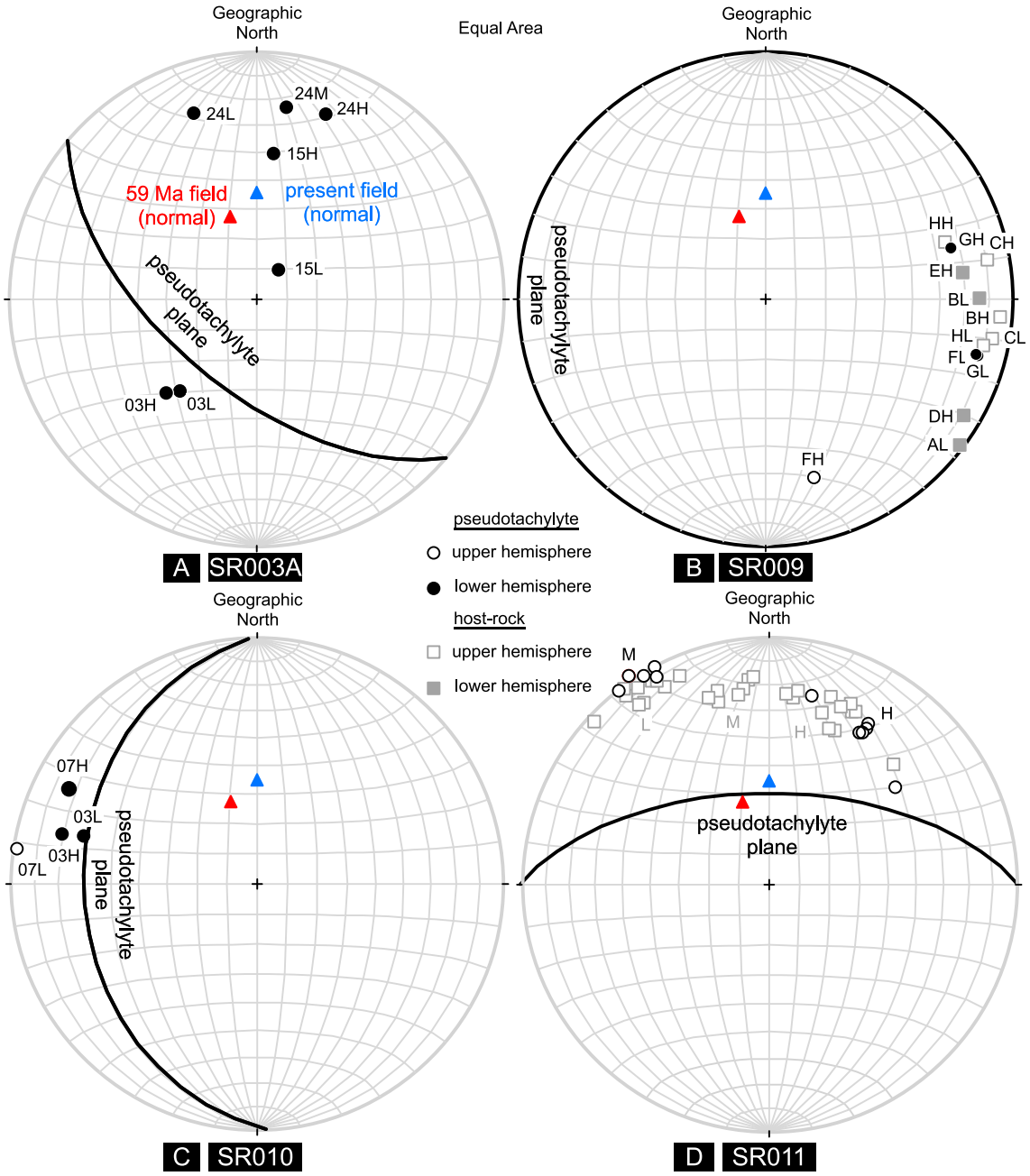


**Figure 15.** Stereonets of NRM demagnetization directions of geographically oriented specimens SR003A, SR009, SR010, and SR011. Data presented in the specimen framework (uncorrected). The pseudotachylyte plane is shown as a great circle. The present-time averaged magnetic dipole field (in blue) and 59 Ma averaged magnetic dipole field (in red) are shown as triangles. Labels indicate the number of individual specimens, while L, M, and H refer to a low-, medium- and high-temperature components, respectively.

However, we note that the Santa Rosa pseudotachylytes formed at a depth of about 7–10 km, which is greater than the typical setting of studies that report the presence of goethite or maghemite. Presumably, at Santa Rosa, coseismic meteoric fluids were neither sufficiently abundant nor oxidizing enough for the growth of either of these two phases. *O'Hara and Sharp* [2001] and *Moecher and Sharp* [2004] showed, using stable isotope data, that meteoric waters are typically not involved in frictional melting. Finally, the presence of grey, coarse (up to 7 mm) specular hematite crystals along contacts between the vein and the host rock [*Ferré et al.*, 2005b, 2012] proves the late stage, postseismic origin of this hematite. This oxidation may have taken place during the uplift of units.

The zonation in the magnetic assemblages observed across pseudotachylyte veins, with hematite-rich rims and hematite-poor centers (Figures 4 and 6–8), emphasizes the importance of performing magnetic measurements preferably on fresh veins and, preferably, on material from the center of the vein. The low thermal stability of oxidized assemblages, such as those represented in Figures 7 (specimen A) and 8 (specimen A), constitute another reason to avoid oxidized parts of pseudotachylyte veins. Despite the significant change in magnetic assemblage, the NRM (Figures 10–12) remains high across pseudotachylyte veins. The high NRM intensities, along with the systematic decrease in magnetic susceptibility observed on magnetic maps of slabs [*Ferré et al*., 2012] (Figure 4), are attributed to both the high magnetite concentration in the vein and the small grain size resulting in higher magnetic remanence. Enhanced NRM intensity in pseudotachylytes and nonpseudotachylyte fault rocks compared to their host rock has been reported in several studies [e.g., *Nakamura and Nagahama*, 2001; *Fukuchi*, 2003; *Hirono et al*., 2006; *Chou et al*., 2012]. In most cases, authors attribute the NRM increase to a change in mineralogy resulting from a temperature increase [e.g., *Fukuchi et al*., 2005; *Tanikawa et al*., 2008]. In some cases, $\delta^{18}O$ isotopic data support the hypothesis that dehydration of hydrous phases controlled the reactions involving magnetic minerals [*O'Hara and Sharp*, 2001].

The mass-normalized NRM intensity varies over 3 orders of magnitude along some pseudotachylyte generation veins (Figure 9a) while it remains relatively consistent in other cases (Figure 9b). The large variations cannot be attributed to variations in saturation remanent magnetization ($M_r$), i.e., concentration of magnetite, because $M_r$ remains relatively constant along veins. These variations cannot be attributed either to selective alteration of the vein because nearby specimens display nearly identical NRM demagnetization behaviors yet large differences in NRM intensity. The observed large variations in NRM must be related to changes in the efficiency of the magnetization process or the intensity of the magnetizing field.

The characteristic magnetizations isolated in progressive demagnetization of the unaltered and the oxidized parts of pseudotachylyte veins at the Santa Rosa locality shed light on whether oxidation took place during or after seismic slip. The distinctly different directions of magnetizations contained in oxidized and unaltered specimens of sample SR031 (Figure 8) and SR012 (Figure 13) are here interpreted to suggest that alteration-related magnetization acquisition took place long after the earthquake. The coseismic magnetic assemblage observed in the pseudotachylytes of Santa Rosa is consistent with formation at intermediate crustal depths where magnetite generally dominates [e.g., *Piper*, 1981; *Nakamura and Nagahama*, 2001; *Davidson et al*., 2003]. In contrast, pseudotachylytes formed at greater depths tend to be ilmenite dominated [e.g., *Austrheim and Boundy*, 1994; *Zechmeister et al*., 2007], while pseudotachylytes that formed at shallower depths commonly exhibit coseismically formed maghemite or hematite [e.g., *Fukuchi*, 2003; *Petrik et al*., 2003]. Factors such as lithology and degree of melting also affect oxygen fugacity and therefore can result in different magnetic assemblages [*Henkel and Reimold*, 2002; *Nakamura and Iyeda*, 2005; *Hirono et al*., 2006].

During cooling of a melt, a pseudotachylyte vein should acquire a primary thermal remanent magnetization (TRM), which may be eventually modified by a secondary chemical remanent magnetization (CRM) caused by meteoric fluid alteration [*Molina Garza et al*., 2009; *Ferré et al*., 2012]. However, the magnetization intensity of some Santa Rosa pseudotachylyte veins varies significantly along the generation vein plane (Figure 9). This variation in part reflects the volume of pseudotachylyte material in the specimen. For example, specimen SR003A24 (NRM = $23.0 \cdot 10^{-6}$ $Am^2/kg$) contains about 50% in volume of pseudotachylyte, whereas SR003A03 (NRM = $4.89 \cdot 10^{-6}$ $Am^2/kg$) is 100% pseudotachylyte (Tables 3 and 4). However, the twice higher magnetite concentration in the pseudotachylyte-rich specimen cannot account for the 2 orders of magnitude difference in NRM between these two specimens.

Sample SR003A yielded specimens that display contrasted behaviors: SR003A03 with a very high NRM intensity and SR003A24 with a low NRM intensity. These two specimens also display nearly orthogonal components and different responses to thermal demagnetization (Figures 9a and 15a). Specimen SR003A15, situated in between SR003A03 and SR003A24, displays two components of stable magnetization each corresponding to the directions of its adjacent specimens. The configuration of these three specimens suggests that SR003A03 and SR003A24 recorded two different magnetization events and that SR003A15 recorded both. The reason that the hematite-born (HT) component of SR003A3 and SR003A24 are distinct remains unclear.

**Table 3.** Thermal Demagnetization Experiments of the Santa Rosa Pseudotachylytes and Host Rocks[a]

| | Host Rocks | | | | | | | Pseudotachylite | | | | |
|---|---|---|---|---|---|---|---|---|---|---|---|---|
| Sample | 010-C6 | 010-F7 | 010-F2 | 010-H3 | 010-G4 | 010-D2 | 010-B4 | 003A-03 | 003A-15 | 003A-24 | 010-E7 | 010-E3 |
| NRM (A/m) | 0.019 | 1.664 | 0.937 | 0.216 | 0.077 | 0.136 | 0.028 | 132.200 | 0.030 | 0.627 | 6.770 | 3.038 |
| *T*°C | | | | | | | | | | | | |
| 25 | 100.0 | 100.0 | 100.0 | 100.0 | 100.0 | 100.0 | 100.0 | 100 | 100 | 100 | 100 | 100 |
| 80 | 81.7 | 101.7 | 91.0 | 93.5 | 88.6 | 80.9 | 98.9 | 96 | 89 | 96 | 97 | 94 |
| 140 | 52.7 | 82.8 | 78.2 | 82.6 | 75.5 | 57.8 | 108.8 | 81 | 75 | 96 | 95 | 84 |
| 210 | 35.4 | 79.1 | 76.4 | 78.8 | 71.9 | 57.4 | 83.4 | 73 | 68 | 96 | 93 | 83 |
| 300 | 28.9 | 75.6 | 72.9 | 69.0 | 71.3 | *32.5* | 61.8 | 60 | 60 | 96 | 94 | 81 |
| 380 | 26.3 | 66.5 | 69.7 | 64.2 | 69.5 | 40.9 | 50.5 | 49 | 57 | 95 | 90 | 76 |
| 440 | *32.0* | 62.9 | 67.1 | 60.3 | 64.9 | 38.2 | *52.7* | 43 | 53 | 95 | 88 | 73 |
| 490 | *32.6* | 59.6 | 60.3 | 50.6 | 55.2 | 36.3 | 40.6 | 35 | 49 | 85 | 86 | 69 |
| 520 | *36.7* | 48.8 | 44.5 | 41.5 | 46.6 | 32.6 | 38.2 | 29 | 40 | 77 | 81 | 60 |
| 540 | *28.8* | 14.9 | 32.2 | 35.4 | 34.3 | 20.1 | *49.8* | 15 | 32 | 67 | 35 | 21 |
| 555 | *37.4* | 9.1 | 17.5 | 23.1 | 31.3 | 16.9 | 34.5 | 13 | 27 | 47 | 34 | 11 |
| 562 | *35.9* | 7.9 | 13.8 | 22.7 | *31.6* | 16.0 | *43.1* | 10 | 30 | 22 | 33 | 8 |
| 570 | 4.7 | 5.2 | 10.2 | 19.1 | *32.2* | 15.1 | *35.3* | 8 | 27 | 16 | 10 | 6 |
| 580 | *18.0* | 3.1 | | 6.7 | 10.1 | 8.9 | *41.7* | 4 | 19 | 6 | 2 | 2 |
| 595 | | 0.9 | | *0.6* | 7.9 | 6.0 | 32.6 | 3 | 16 | 3 | 1 | 1 |
| 610 | | 0.3 | | 1.3 | *8.7* | *5.2* | 22.9 | 0 | 15 | 2 | 0 | 0 |
| 630 | | 0.3 | | 1.0 | *11.8* | *6.2* | 15.1 | 0 | 15 | 1 | 0 | 0 |
| 650 | | 0.3 | | | | *7.3* | 12.9 | 0 | 14 | 1 | 0 | 1 |
| 665 | | 0.2 | | | | 4.9 | | 0 | 12 | 0 | 0 | |

[a]Numbers in italic indicate inverse component.

**Table 4.** NRM Intensities of the Santa Rosa Pseudotachylytes and Host Rocks

| Sample | Pseudotachylytes(10-6 $Am^2/kg$) | Sample | Host Rocks(10-6 $Am^2/kg$) |
|---|---|---|---|
| SR003A03 | 4891.00 | SR009A | 3.85 |
| SR003A15 | 1.11 | SR009B | 2.08 |
| SR003A24 | 23.00 | SR009C | 116.00 |
| SR009 F | 2977.00 | SR009D | 229.00 |
| SR009G | 1885.00 | SR009E | 290.00 |
| SR010-03 | 251.00 | SR009H | 39.60 |
| SR010-07 | 113.00 | SR011A | 5.01 |
| SR011C | 122.00 | SR011B | 12.00 |
| SR011D | 138.00 | SR011I | 20.60 |
| SR011E | 133.00 | SR011J | 8.85 |
| SR011F | 108.90 | SR011K | 3.83 |
| SR011G | 126.00 | SR011L | 3.94 |
| SR011H | 117.00 | SR011M | 5.02 |
| SR012A | 372.00 | SR011N | 0.87 |
| SR012B | 630.00 | SR011O | 0.96 |
| SR031A | 6720.00 | SR011P | 1.13 |
| SR031B | 5920.00 | SR011Q | 3.11 |
| SR034 | 3261.00 | SR045A | 1.04 |
| SR045D | 15.40 | SR045B | 3.66 |
| SR045E | 47.00 | SR045C | 3.43 |
| SR045F | 92.50 | SR045H | 4.43 |
| SR045G | 10.60 | SR045I | 2.80 |
| | | SR045J | 6.39 |
| | | SR045K | 13.30 |
| | | SR045L | 17.50 |
| | | SR045M | 6.67 |
| | | SR045N | 6.11 |
| | | SR045O | 3.67 |
| Average | 1270.66 | | 29.10 |

In order to elucidate certain aspects of pseudotachylyte paleomagnetic record, we performed thermal demagnetization experiments on specimens obtained along transects across veins (Figures 10–12). All transects show a higher NRM intensity in the pseudotachylyte vein compared to the host rock (average host rock NRM = $29.0 \cdot 10^{-6}$ $Am^2/kg$; average pseudotachylyte NRM = $1270 \cdot 10^{-6}$ $Am^2/kg$). The thermal demagnetization behavior of pseudotachylytes is systematically characterized by higher laboratory unblocking temperatures than the host rock, which is consistent with low-Ti magnetite as the principal remanence carrier. Pseudotachylytes are also characterized by two stable NRM components: a low-blocking temperature (LT) component (<550°C) interpreted to be carried by magnetite and a high-blocking temperature (HT) component carried by hematite (>550°C). The directions of each component are consistent within each transect. The LT NRM component is interpreted as a TRM, and the HT component is interpreted as a CRM.

Quenched melts should constitute an excellent material for paleointensity studies because of the high magnetic coercivity of typically noninteracting fine-grained magnetite grains [*Pick and Tauxe*, 1993; *Tarduno et al*., 2001]. Pseudotachylytes would also be expected to act as quality recorders of the geomagnetic field [*Nakamura and Iyeda*, 2005; *Nakamura and Uehara*, 2005], as long as the acquisition of postcooling, meteoric alteration CRMs is insignificant.

At the Santa Rosa Deep Canyon sampling site (33°34′N, 116°25′W), the present-day geomagnetic field direction has a declination $D = 11.9°$, an inclination $I = +58.9°$, and an intensity of 47,300 nT (International Geomagnetic Reference Field 2011 Model). At the time of seismic slip, 59 Ma ago, the time averaged normal polarity geocentric axial dipole paleomagnetic field direction was about $D = 342°$ and $I = +61°$, based on the compilation of *Torsvik et al*. [2012] (their Table 2, spline 300, Qf = 0.6, poles for Laurentia).

The three main characteristics of the oriented specimens are (Figure 15) (1) NRM components lie away from both present- and 59 Ma-time averaged magnetic dipole fields, (2) pseudotachylyte and host rock share similar components, and (3) the NRM components of transects SR009 and SR011 display girdle distributions.

Considering the high frictional heat produced during seismic slip along the generation vein, the host rock must have been remagnetized at a short distance from the pseudotachylyte vein, in a manner similar to the baked contact of an intrusive. We interpret the high-temperature component of the NRM in the pseudotachylyte veins and their host rock to correspond to TRM acquired by magnetite SD-PSD grains upon cooling in the geomagnetic field at 59 Ma. The postseismic alteration of pseudotachylytes by meteoric fluids would have then imparted a CRM component distinct from the TRM directions. However, the angular difference between TRM and CRM observed on altered specimens (Figures 8 and 13) is significantly larger (≥36°) than the change in time average magnetic dipole direction between 59 Ma and the present (13°, from $D = 342°$, $I = +61°$ at 59 Ma to $D = 0°$, $I = 53°$ at the present). Post-Paleocene block rotation in the Santa Rosa Mountains is likely because this area, located between the San Jacinto Fault and the San Andreas Fault, is tectonically very active [e.g., *Bennett et al*., 2004]. This deformation could explain the angular difference between the TRM and CRM components and why all components are away from the 59 Ma field. The SR009 and SR011 girdle distributions require a specific remanence acquisition process. The anisotropic acquisition of remanence, a common phenomenon in sediments [e.g., *Tan and Kodama*, 2002], cannot explain girdles because it would require a similar preferred orientation of ferromagnetic grains in the pseudotachylyte vein and the host rock. Clearly, the fabric of the host rock has not been modified by seismic slip. Alternatively, ductile shearing of the host rock/pseudotachylyte vein system would produce two drag folds on the flanks of the pseudotachylyte, which in turn could cause synmagnetization folding. However, the lack of pervasive postsolidification ductile or brittle strain in the host rock does not support this explanation. We propose that the transfer of heat from the pseudotachylyte to its host rock resulted in a baked contact aureole. With this model, as the distance to the vein decreases, the Cretaceous TRM of the host rock is gradually replaced by the Paleocene TRM of the pseudotachylyte vein.

The possibility that some anomalous magnetization directions observed in the oriented transects results from coseismic electromagnetic phenomena such as earthquake lightnings [*Enomoto and Zheng*, 1998; *Ferré et al*., 2005b] cannot be excluded. Since the pseudotachylytic melt has an electrical conductivity substantially higher than that of the host rock, coseismic electrical currents have to travel along a specific line within the plane of the generation vein. Regardless of the specific orientation of this line, the magnetic field resulting from the coseismic current would have to be perpendicular to the generation vein and would impart an isothermal

remanent magnetization (IRM) to rocks nearby. The IRM component would in most cases be anomalous with respect to the geomagnetic field. In some cases, close to the coseismic lightning path, the IRM might also be anomalous in intensity.

## 8. Conclusions

The NRM of the Santa Rosa pseudotachylytes consists essentially of a TRM carried by PSD-SD magnetite grains and acquired upon cooling of the vein. It is superimposed by a CRM carried by hematite and acquired long after seismic slip through alteration by meteoric fluids. The TRM of the pseudotachylyte and the NRM of its host rock potentially hold clues to the thermal conditions of seismic slip in the vein and in the host rock at the time of the earthquake. In addition, the determination of the intensity and direction of the primary magnetization acquired by the Santa Rosa pseudotachylytes shows that they portray coseismic conditions. In the pseudotachylyte veins, the low laboratory unblocking temperature magnetizations have intensities and directions that are clearly distinct from those of the host rock. We interpret this difference as resulting primarily from a distinct magnetization process related to the seismic slip event and the rapid quenching of the melt. At Santa Rosa, the coseismic paleomagnetic record of pseudotachylytes does not seem to have been overprinted by postseismic thermal events.

**Acknowledgments**

This research was funded through NSF grants EAR0228818 (Ferré), EAR0228849 (Geissman), and EAR0521558 (Ferré). We thank Jason Rampe for his assistance in collecting samples in the field. Steve Harlan is thanked for performing thermomagnetic experiments on the CS3-KLY-3S furnace at George Mason University. M.J.H. acknowledges NERC grant NE/I013873/1. The paleomagnetic and rock magnetic data are available through the Paleomagnetic Database, an online portal to the archives of the Magnetics Information Consortium (MagIC, http://earthref.org/magic) that contains both paleomagnetic and rock magnetic data. Three anonymous reviewers provided very insightful comments on this work and are gratefully acknowledged.

## References

Abercrombie, R., A. McGarr, H. Kanamori, and G. Di Toro (2006), *Earthquakes: Radiated Energy and the Physics of Faulting*, 327 pp., AGU, Washington, D. C.

Andersen, T. B., and H. Austrheim (2006), Fossil earthquakes recorded by pseudotachylytes in mantle peridotite from the Alpine subduction complex of Corsica, *Earth Planet. Sci. Lett.*, *242*, 58–72.

Austrheim, H., and T. M. Boundy (1994), Pseudotachylytes generated during seismic faulting and eclogitization of the deep crust, *Science*, *265*, 82–83.

Beckmann, G. E. J. (1982), Palaeomagnetism of some Precambrian rocks in south-east Greenland, *Phys. Earth Planet. Inter.*, *32*, 85–99.

Belley, F., E. C. Ferré, F. Martin-Hernandez, M. J. Jackson, M. D. Dyar, and E. J. Catlos (2009), The magnetic properties of natural and synthetic $(Fe_x, Mg_{1-x})_2$ $SiO_4$ olivines, *Earth Planet. Sci. Lett.*, *284*(3–4), 516–526.

Bennett, R. A., A. M. Friedrich, and K. P. Furlong (2004), Codependent histories of the San Andreas and San Jacinto fault zones from inversion of fault displacement rates, *Geology*, *32*(11), 961–964.

Chou, Y.-M., S.-R. Song, C. Aubourg, T.-Q. Lee, A.-M. Boullier, Y.-F. Song, E.-C. Yeh, L.-W. Kuo, and C.-Y. Wang (2012), An earthquake slip zone is a magnetic recorder, *Geology*, *40*(6), 551–554.

Coe, R. S. (1967), Paleointensities of the Earth's magnetic field determined from Tertiary and Quaternary rocks, *J. Geophys. Res.*, *72*(12), 3247–3262, doi:10.1029/JZ072i012p03247.

Davidson, C., K. J. Davis, C. M. Bailey, C. H. Tape, J. Singleton, and B. Singer (2003), Age, origin, and significance of brittle faulting and pseudotachylyte along the coast shear zone, Prince Rupert, British Columbia, *Geology*, *31*(1), 43–46.

Day, R., M. Fuller, and V. A. Schmidt (1977), Hysteresis properties of titanomagnetites: Grain-size and compositional dependence, *Phys. Earth Planet. Inter.*, *13*, 260–267.

Del Gaudio, P., G. Di Toro, R. Han, T. Hirose, S. Nielsen, T. Shimamoto, and A. Cavallo (2009), Frictional melting of peridotite and seismic slip, *J. Geophys. Res.*, *114*, B06306, doi:10.1029/2008JB005990.

Di Toro, G., S. Nielsen, and G. Pennachioni (2005), Earthquake rupture dynamics frozen in exhumed ancient faults, *Nature*, *436*, 1009–1012.

Enomoto, Y., and Z. Zheng (1998), Possible evidences of earthquake lightning accompanying the 1995 Kobe earthquake inferred from the Nojima fault gouge, *Geophys. Res. Lett.*, *25*(14), 2721–2724, doi:10.1029/98GL02015.

Ferré, E. C., J. L. Allen, and A. Lin (2005a), Pseudotachylytes and seismogenic friction: An introduction to current research, *Tectonophysics*, *402*(1–4), 1–2.

Ferré, E. C., M. S. Zechmeister, J. W. Geissman, N. MathanaSekaran, and K. Kocak (2005b), The origin of high magnetic remanence in fault pseudotachylites: Theoretical considerations and implication for coseismic electrical currents, *Tectonophysics*, *402*(1–4), 125–139.

Ferré, E. C., J. W. Geissman, and M. S. Zechmeister (2012), Magnetic properties of fault pseudotachylytes in granites, *J. Geophys. Res.*, *117*, B01106, doi:10.1029/2011JB008762.

Fukuchi, T. (2003), Strong ferrimagnetic resonance signal and magnetic susceptibility of the Nojima pseudotachylyte in Japan and their implication for coseismic electromagnetic changes, *J. Geophys. Res.*, *108*(B6), 2312, doi:10.1029/2002JB002007.

Fukuchi, T., K. Mizoguchi, and T. Shimamoto (2005), Ferrimagnetic resonance signal produced by frictional heating: A new indicator of paleoseismicity, *J. Geophys. Res.*, *110*, B12404, doi:10.1029/2004JB003485.

Gattacceca, J., and P. Rochette (2004), Toward a robust normalized magnetic paleointensity method applied to meteorites, *Earth Planet. Sci. Lett.*, *227*(3–4), 377–393.

Goodwin, L. B., and P. R. Renne (1991), Effects of progressive mylonitization on Ar retention in biotites from the Santa Rosa Mylonite Zone, California, and thermochronologic implications, *Contrib. Mineral. Petrol.*, *108*, 283–297.

Grocott, J. (1981), Fracture geometry of pseudotachylyte generation zones: A study of shear fractures formed during seismic events, *J. Struct. Geol.*, *3*(2), 169–178.

Harrison, R. J., and J. M. Feinberg (2008), FORCinel: An improved algorithm for calculating first-order reversal curve distributions using locally weighted regression smoothing, *Geochem. Geophys. Geosyst.*, *9*, Q05016, doi:10.1029/2008GC001987.

Henkel, H., and W. U. Reimold (2002), Magnetic model of the central uplift of the Vredefort impact structure, South Africa, *J. Appl. Geophys.*, *51*(1), 43–62.

Hill, M. J., and J. Shaw (2000), Magnetic field intensity study of the 1960 Kilauea lava flow, Hawaii, using the microwave palaeointensity technique, *Geophys. J. Int.*, *142*(2), 487–504.

Hill, M. J., J. Shaw, and E. Herrero-Bervera (2006), Determining palaeointensity from the Gilbert Gauss Reversal recorded in the Pu,Äôu Heleakala lava section, Wai,Äôanae Volcano, Oahu, *Earth Planet. Sci. Lett.*, *245*(1–2), 29–38.

Hirono, T., et al. (2006), Evidence of frictional melting from disk-shaped black material, discovered within the Taiwan Chelungpu fault system, *Geophys. Res. Lett.*, *33*, L19311, doi:10.1029/2006GL027329.
Janssen, C., R. Wirth, E. Rybacki, R. Naumann, H. Kemnitz, H. R. Wenk, and G. Dresen (2010), Amorphous material in SAFOD core samples (San Andreas Fault): Evidence for crush-origin pseudotachylytes?, *Geophys. Res. Lett.*, *37*, L01303, doi:10.1029/2009GL040993.
Kirkpatrick, J. D., Z. K. Shipton, and C. Persano (2009), Pseudotachylytes: Rarely generated, rarely preserved, or rarely reported?, *Bull. Seismol. Soc. Am.*, *99*(1), 382–388, doi:10.1785/0120080114.
Lin, A. (2008), *Fossil Earthquakes: The Formation and Preservation of Pseudotachylytes*, 345 pp., Springer, Berlin, Germany.
Lin, A. (2011), Seismic slip recorded by fluidized ultracataclastic veins formed in a coseismic shear zone during the 2008 Mw 7.9 Wenchuan earthquake, *Geology*, *39*(6), 547–550, doi:10.1130/g32065.1.
Maddock, R. H. (1983), Melt origin of pseudotachylites demonstrated by textures, *Geology*, *11*, 105–108.
Magloughlin, J. F. (1992), Microstructural and chemical changes associated with cataclasis and frictional melting at shallow crustal levels: The cataclasite-pseudotachylyte connection, *Tectonophysics*, *204*, 243–260.
Martín-Hernández, F., and E. C. Ferré (2007), Separation of paramagnetic and ferrimagnetic anisotropies: A review, *J. Geophys. Res.*, *112*, B03105, doi:10.1029/2006JB004340.
Moecher, D. P., and Z. D. Sharp (2004), Stable isotope and chemical systematics of pseudotachylyte and wall rock, Homestake shear zone, Colorado, USA: Meteoric fluid or rock-buffered conditions during coseismic fusion?, *J. Geophys. Res.*, *109*, B12206, doi:10.1029/2004JB003045.
Molina Garza, R. S., J. Geissman, T. Wawrzyniec, B. Weber, M. López Martínez, and J. Aranda-Gómez (2009), An integrated magnetic and geological study of cataclasite-dominated pseudotachylytes in the Chiapas Massif, Mexico: A snapshot of stress orientation following slip, *Geophys. J. Int.*, *177*(3), 891–912.
Muxworthy, A., and A. P. Roberts (2007), First-order reversal curve (FORC) diagrams, in *Encyclopedia of Geomagnetism and Paleomagnetism*, edited by D. Gubbins and E. Herrero-Bervera, pp. 266–272, Springer, Berlin, Germany.
Nakamura, N., and H. Nagahama (2001), Changes in magnetic and fractal properties of fractured granites near the Nojima Fault, Japan, *Island Arc*, *10*, 486–494.
Nakamura, N., and M. Uehara (2005), Pseudotachylyte and chondrule as a reliable recorder of ancient magnetic field (in Japanese), *J. Geogr.*, *114*(2), 223–238.
Nakamura, N., and Y. Iyeda (2005), Magnetic properties and paleointensity of pseudotachylytes from the Sudbury structure, Canada: Petrologic control, *Tectonophysics*, *402*(1–4), 141–152.
Nakamura, N., T. Hirose, and G. J. Borradaile (2002), Laboratory verification of submicron magnetite production in pseudotachylytes: Relevance for paleointensity studies, *Earth Planet. Sci. Lett.*, *201*, 13–18.
Niemeijer, A., G. Di Toro, W. A. Griffith, A. Bistacchi, S. A. F. Smith, and S. Nielsen (2013), Inferring earthquake physics and chemistry using an integrated field and laboratory approach, *J. Struct. Geol.*, *39*(0), 2–36.
O'Hara, K. D., and Z. D. Sharp (2001), Chemical and oxygen isotope composition of natural and artificial pseudotachylyte: Role of water during frictional fusion, *Earth Planet. Sci. Lett.*, *184*(2), 393–406.
Petrik, I., P. I. Nabelek, M. Janak, and D. Plasienka (2003), Conditions of formation and crystallization kinetics of highly oxidized pseudotachylytes from the High Tatras (Slovakia), *J. Petrol.*, *44*(5), 901–927.
Pick, T. S., and L. Tauxe (1993), Geomagnetic palaeointensities during the Cretaceous normal superchron measured using submarine basaltic glass, *Nature*, *366*, 238–242.
Pike, C. R., A. P. Roberts, and K. L. Verosub (1999), Characterizing interactions in fine magnetic particle systems using first order reversal curves, *J. Appl. Phys.*, *85*(9), 6660–6667.
Piper, J. D. A. (1981), Palaeomagnetism of pseudotachylites from the Ikertôk shear belt, and their relationship to the kimberlite-lamprophyre province, central-west Greenland, *Bull. Geol. Soc. Den.*, *30*, 57–67.
Piper, J. D. A., and T. J. Poppleton (1988), Palaeomagnetic dating of pseudotachylyte formation in the Lewisian complex, *Scott. J. Geol.*, *24*(3), 263–272.
Roberts, A. P., C. R. Pike, and K. L. Verosub (2000), First-order reversal curve diagrams: A new tool for characterizing the magnetic properties of natural samples, *J. Geophys. Res.*, *105*(B12), 28,461–28,475, doi:10.1029/2000JB900326.
Rowe, C. D., A. Fagereng, J. A. Miller, and B. Mapani (2012), Signature of coseismic decarbonation in dolomitic fault rocks of the Naukluft Thrust, Namibia, *Earth Planet. Sci. Lett.*, *333*(3–4), 200–210.
Shaw, J. (2007), Microwave paleomagnetic technique, in *Encyclopedia of Geomagnetism and Paleomagnetism*, edited by D. Gubbins and E. Herrero-Bervera, pp. 694–695, Springer, Netherlands.
Spray, J. G. (2011), Frictional melting processes in planetary materials: From hypervelocity impact to earthquakes, *Annu. Rev. Earth Planet. Sci.*, *38*(1), 221–254.
Tan, X., and K. P. Kodama (2002), Magnetic anisotropy and paleomagnetic inclination shallowing in red beds: Evidence from the Mississippian Mauch Chunk Formation, Pennsylvania, *J. Geophys. Res.*, *107*(B11), 2311, doi:10.1029/2001JB001636.
Tanikawa, W., T. Mishima, T. Hirono, W. Soh, and S.-R. Song (2008), High magnetic susceptibility produced by thermal decomposition of core samples from the Chelungpu fault in Taiwan, *Earth Planet. Sci. Lett.*, *272*(1–2), 372–381.
Tarduno, J. A., R. D. Cottrell, and A. V. Smirnov (2001), High geomagnetic intensity during the Mid-Cretaceous from Thellier analyses of single plagioclase crystals, *Science*, *291*(5509), 1779–1783, doi:10.1126/science.1057519.
Techmer, K. S., H. Ahrendt, and K. Weber (1992), The development of pseudotachylyte in the Ivrea-Verbano Zone of the Italian Alps, *Tectonophysics*, *204*(3–4), 307–322.
Techmer, K. S., C. Echer, and H. R. Wenk (1996), SEM and TEM/AEM studies of crystallization processes in some natural glasses (Pseudotachylites of the Ivrea-Verbano zone, Northern Italy and Quenched Volcanic rocks from Mono Lake, California), *Chemie der Erde, Geochem.*, *56*, 373–378.
Thellier, E., and O. Thellier (1959), Sur l'intensité du champ magnétique terrestre dans le passé historique et géologique, *Ann. Geophys.*, *15*, 285–378.
Torsvik, T. H., et al. (2012), Phanerozoic polar wander, palaeogeography and dynamics, *Earth Sci. Rev.*, *114*(3–4), 325–368.
Ueda, T., M. Obata, G. Di Toro, K. Kanagawa, and K. Ozawa (2008), Mantle earthquakes frozen in mylonitized ultramafic pseudotachylytes of spinel-lherzolite facies, *Geology*, *36*(8), 607–610, doi:10.1130/g24739a.1.
Walton, D., J. Share, T. C. Rolph, and J. Shaw (1993), Microwave magnetization, *Geophys. Res. Lett.*, *20*, 109–111, doi:10.1029/92GL02782.
Wenk, H. R., L. R. Johnson, and L. Ratschbacher (2000), Pseudotachylites in the Eastern Peninsular Ranges of California, *Tectonophysics*, *321*, 253–277.
Zechmeister, M. S., E. C. Ferré, M. A. Cosca, and J. W. Geissman (2007), Slow and fast deformation in the Dora Maira Massif, Italian Alps: Pseudotachylytes and inferences on exhumation history, *J. Struct. Geol.*, *29*(7), 1114–1130.
Zijderveld, J. A. C. (1967), Demagnetization of rocks: Analysis of results, in *Methods in Paleomagnetism*, edited by D. W. Collinson, K. M. Creer, and S. K. Runcorn, pp. 254–286, Elsevier, Amsterdam, Netherlands.